Sippel, J., Fuchs, S., Cacace, M., Kastner, O., Huenges, E., Scheck-Wenderoth, M. (2013): Deep 3D thermal modelling for the city of Berlin (Germany). - *Environmental Earth Sciences*, *70*, 8, 3545-3566

DOI: 10.1007/s12665-013-2679-2

„Deep 3D thermal modeling for the city of Berlin (Germany) “

This paper was originally published in:

Environmental Earth Sciences [Springer], July 2013, „ Deep 3D thermal modeling for the city of Berlin (Germany) “

doi: 10.1007/s12665-013-2679-2

The final publication is available at:

http://link.springer.com/article/10.1007%2Fs12665-013-2679-2

Received: 22.11.2012

Accepted: 15.07.2013

Published online: 28.07.2013

Authors

Dr. Judith Sippel, Sven Fuchs, Dr. Mauro Cacace , Anna Braatz, Dr. Oliver Kastner, Dr. Ernst Huenges
Dr. Magdalena Scheck-Wenderoth

Affiliations

J. Sippel (corresponding author)
GeoForschungsZentrum Potsdam (GFZ), Telegrafenberg, D-14773, Potsdam, Germany
Tel.: +49-331-2881342
Fax: +49-331-2881349
E-mail: sippel@gfz-potsdam.de

S. Fuchs, GeoForschungsZentrum Potsdam (GFZ), Telegrafenberg, D-14773, Potsdam, Germany
M. Cacace, GeoForschungsZentrum Potsdam (GFZ), Telegrafenberg, D-14773, Potsdam, Germany
A. Braatz, Wintershall Holding GmbH, EXX - New Exploration Opportunities , D-34119 Kassel, Germany
O. Kastner, GeoForschungsZentrum Potsdam (GFZ), Telegrafenberg, D-14773, Potsdam, Germany
E. Huenges, GeoForschungsZentrum Potsdam (GFZ), Telegrafenberg, D-14773, Potsdam, Germany
M. Scheck-Wenderoth, GeoForschungsZentrum Potsdam (GFZ), Telegrafenberg, D-14773, Potsdam, Germany

Abstract

This study predicts the subsurface temperature distribution of Germany's capital Berlin. For this purpose, a data-based lithosphere-scale 3D structural model is developed incorporating 21 individual geological units. This model shows a horizontal grid resolution of (500 x 500) m and provides the geometric base for two different approaches of 3D thermal simulations, (i) calculations of the steady-state purely conductive thermal field and (ii) simulations of coupled fluid flow and heat transport.

The results point out fundamentally different structural and thermal configurations for potential geothermal target units. The top of the Triassic Middle Buntsandstein strongly varies in depth (159-2,470 m below sea level) and predicted temperatures (15-95°C), mostly because of the complex geometry of the underlying Permian Zechstein salt. The top of the sub-salt Sedimentary Rotliegend is rather flat (2,890-3,785 m below sea level) and reveals temperatures of 85-139°C. The predicted 70°C-isotherm is located at depths of about 1,500-2,200 m cutting the Middle Buntsandstein over large parts of Berlin. The 110°C-isotherm at 2,900-3,700 m depth widely crosscuts the Sedimentary Rotliegend.

Groundwater flow results in subsurface cooling the extent of which is strongly controlled by the geometry and the distribution of the Tertiary Rupelian Clay. The cooling effect is strongest where this clay-rich aquitard is thinnest or missing thus facilitating deep reaching forced convective flow. The differences between the purely conductive and coupled models highlight the need for investigations of the complex interrelation of flow- and thermal fields to properly predict temperatures in sedimentary systems.

Keywords: 3D geological model, conductive thermal field, coupled fluid and heat transport, Energy Atlas Berlin

1 Introduction

Energy consumption is one of the largest contributors to CO_2 emissions, one of the most talked causes of climate change. Big, industrialised and densely populated cities have the biggest share in the world's energy consumption. Almost 80% of the global CO_2 (plus an additional big portion of other greenhouse gases) are emitted from the world's (mega)cities and urban areas (FIG Commission 3, 2010). In the light of an aspired reduction of CO_2 emission to the atmosphere, efficient remedial actions must be taken for carbon dioxide emission reduction.

A city may be considered as an open thermodynamic system continuously utilizing and transforming energy and mass. The objective is to minimise waste production (e.g. including CO_2 and greenhouse gas emissions) and at the same time meeting the internal energy demand. These requirements may be achieved only by minimising the reliance on fossil fuel and by maximizing the use of sustainable and recyclable energy sources. Geothermal energy from hot sedimentary aquifers is recognized as amongst the most cost-effective low-emissions energy sources that can lead the transition towards more environmentally friendly cities (Huenges 2010). This is because geothermal energy has not only applications for electricity generation but also for direct heating.

One example of such an energy demanding city is Berlin, Germany's capital, which the present study focusses on. The total energy consumption of Berlin amounts to about 70 TWh per year of which 40 TWh are used for heating (numbers for the year 2005; Berliner Senatsverwaltung für Wirtschaft, Technologie und Frauen 2011). This demand of energy is still largely (to more than 95%) satisfied by fossil fuels and thus is responsible for significant emissions. The commitment of the Senate of the city to the updated Climate Protection Concept 2020 calls for a new and sustainable energy policy, which should increase the relative share of renewable energy both in gross energy (up to 30%) and electrical consumption (up to 18%). In this respect, the big unknown is how much deep geothermal energy can contribute to these changes.

The city of Berlin is located in the south-eastern domain of the Northeast German Basin (NEGB; Fig. 1), a region that is generally regarded suitable for geothermal exploitation (Agemar et al. 2012). Moreover, the presence of a groundwater system of considerable extent in the shallow subsurface of Berlin (e.g. Jaroch 2006) opens the possibility to deliver the heating and cooling needs of the entire city. However, the temperatures locally observed at several kilometres depth vary considerably across the Berlin area (see below) so that predictions about the city-wide temperature distribution and deep geothermal potential become a challenge.

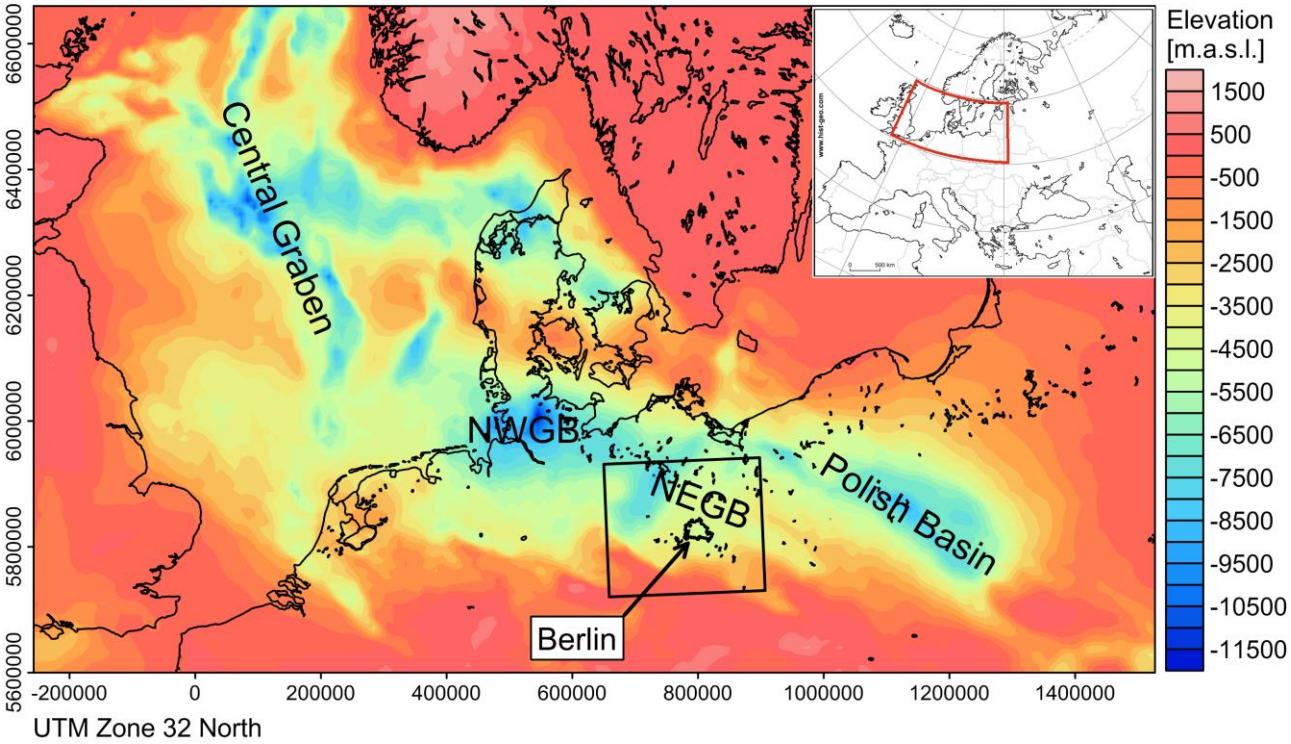

Fig 1 Location of the city of Berlin in the Central European Basin System. Plotted is the depth to the top of Pre-Permian rocks as implemented in the 3D structural model of Scheck-Wenderoth and Lamarche (2005). The rectangle marks the location of the 3D structural model of Brandenburg (Noack et al., 2010, 2012). Abbreviations: NEGB - Northeast German Basin; NWGB - Northwest German Basin; m.a.s.l.: metres above sea level

Previous studies have shown that lateral variations of the thermal field in the NEGB are strongly controlled by the structural configuration of its constituting sediments and crust. For example, subsurface temperatures tend to be larger towards the basin centre where several kilometres of Mesozoic sediments with relatively low thermal conductivity promote heat storage, while the basin margins are efficiently cooled by the highly conductive crystalline crust that reaches much shallower depth (Noack et al. 2010, 2012, 2013 - this issue). In addition, a unit dominated by rock salt (the Upper Permian Zechstein salt), which forms numerous domes and diapirs in the region and is characterised by higher thermal conductivities than the overlying sedimentary sequences, induces significant small-scale thermal anomalies (e.g. Balling et al. 2013 - this issue; Bayer et al. 1997; Cacace et al. 2010; Cherubini et al. 2013 - this issue; Hurtig and Rockel 1992; Noack et al. 2010; Norden et al. 2008). Beside thermal conduction, also heat transfer coupled to flowing groundwater has been identified as an important controlling factor for subsurface temperatures in the NEGB (Cacace et al. 2010; Kaiser et al. 2011; Noack et al. 2013 - this issue).

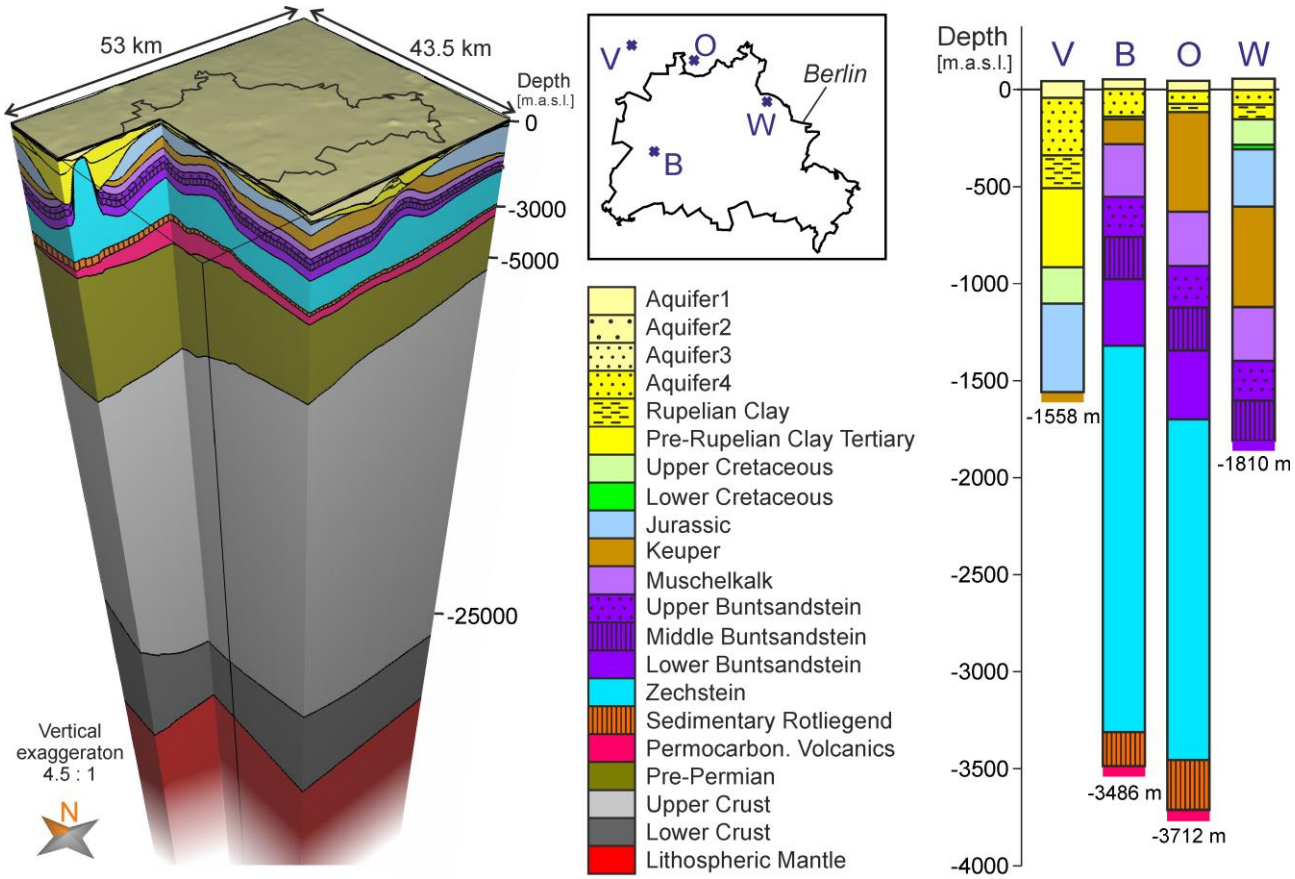

Fig 2 Lithosphere-scale 3D structural model of Berlin with differentiated geological units. Also shown is the stratigraphy at the 4 boreholes and their locations. Note that the lithospheric mantle is not shown with its full vertical extent (i.e. to its maximum depth of 129,598 m.a.s.l.). Abbreviations: B – well E Berlin 1/70 ; O – well E Oranienburg 1/68 ; V – well Gt Velten 2/90 ; W – well Gt Berlin-Wartenberg 2/86; m.a.s.l.: metres above sea level

Considering the complex interplay between crustal structure and temperatures in the NEGB and the limited availability of direct temperature observations for depths greater than 1 km in the Berlin area (Fig. 2), our approach is the following: We combine all available temperature-relevant information with the physics of heat transport in numerical simulations that provide predictions beyond the database. The goal at this stage of geothermal research (prior to drilling) is to obtain as much information about the properties of the city-wide geothermal system as possible. Based on a new 3D geological model of Berlin, numerical simulations of heat transfer – partly connected to groundwater flow – are carried out to predict the subsurface temperature distribution. This requires detailed information on the subsurface distribution of thermal and hydraulic properties, preferably derived from *in-situ* or laboratory measurements. The resulting temperature predictions will help identifying and characterising relevant geological structures of interest for geothermal utilisation, i.e. hot aquifers as a proxy for hydrothermal reservoirs. Moreover, the modelled temperature distribution allows estimating the geothermal potential of deep geological formations in the form of energy density ("heat in place") of the pore fluid and rock matrix (cf. Kastner et al. 2013 - this issue). Any identified warmer domains can at last be the focus of reservoir-scale modelling. This may include simulations of the dynamic behaviour of the hydraulically enhanced reservoir under

specific *in-situ* working conditions, such as already have been performed for the deep geothermal reservoir of Groß Schönebeck (north of Berlin; Blöcher et al. 2010; Wong et al. 2013 - this issue), the city of Den Haag (Mottaghy et al. 2011), and for a fractured carbonate reservoir in the Molasse Basin (Germany; Cacace et al. 2013).

The concept outlined above delineates the major steps of what is usually referred to as a geothermal exploration campaign serving as the scientific guideline for subsequent stages of engineering. In a similar way, temperature predictions based on deterministic geological models and numerical simulations of physical concepts have already shed light on the geothermal potential of the Perth metropolitan area (Schilling et al. 2013) and the city of Den Haag (Mottaghy et al. 2011).

Another challenge is to correlate subsurface information about the geothermal potential to consumer grids. The project "Energy Atlas Berlin" aims to develop "…a holistic decision-making and planning tool to provide integrated assessments of energy demand, energy balancing and planning, based on a virtual 3D city model of Berlin…". Our study on the deep geothermal potential is intended to contribute to this virtual city that also integrates the surface demand and infrastructure to support decision making for a low-carbon urban energy management.

2 Geological setting, previous work and database

The NEGB is a part of the intracontinental Central European Basin System (Fig. 1) of which the present-day structure and past evolution have been studied extensively throughout the last years (e.g. Maystrenko and Scheck-Wenderoth 2013). The development of this complex sedimentary basin system was initiated in Late Carboniferous-Early Permian times with an extensive phase of volcanism documented by the lowermost volcanic rocks of the basin fill (Benek et al. 1996). These volcanic rocks superpose crustal domains of different consolidation ages, Variscan in the Berlin area (Maystrenko and Scheck-Wenderoth 2013). Overlying the volcanics, Permian to Cenozoic sediments attain up to 8,000 m thickness in the NEGB (Scheck and Bayer 1999). The structural configuration of this succession of intercalated clastics and carbonates is strongly modified by the Upper Permian layer of Zechstein salt that has recurrently been mobilised from Mid Triassic times onward (Scheck et al. 2003). After accumulation of an initial thickness of up to 2,500 m in the NEGB (Scheck et al. 2003) and subsequent halokinetic mobilisation during main phases of regional tectonics affecting the entire basin system, the Zechstein salt forms numerous salt diapirs and pillows at present-day, with thicknesses locally exceeding 3,500 m in the NEGB (Maystrenko et al. 2013).

After a Late Cretaceous-Early Tertiary inversion event dominated by uplift and erosion, the Central European Basin System experienced a renewed phase of subsidence with minor fault and salt

tectonic activity during the Cenozoic (Scheck-Wenderoth and Lamarche 2005). The corresponding Tertiary and Quaternary sediments of the NEGB are composed of unconsolidated clastics containing the main aquifer systems partly exploited for the water supply of the city of Berlin. Thereby a lower Oligocene clay-rich formation, the Rupelian Clay, plays an important role in forming a barrier between the Upper Tertiary-Quaternary freshwater aquifers and the deeper saline aquifers (e.g. Noack et al. 2013 - this issue).

Since thermal simulations require well defined thermal and hydraulic properties, knowledge of the present-day subsurface configuration of the main lithological units is a pre-requisite for this study. The 3D geological model for Berlin developed for such simulations builds on a series of regional studies that have already shed light on the structural configuration of the lithosphere. For instance, the 3D structural model of the Central European Basin System (Scheck-Wenderoth and Lamarche 2005) reproduces the present-day configuration of the main Permian to Cenozoic stratigraphic units as indicated by multidisciplinary data (borehole, seismics, outcrop etc.). Later, this regional model was extended to the lithosphere scale by integrating the observed gravity field, seismological data and measured temperatures (Maystrenko and Scheck-Wenderoth 2013). Based on this model, Noack et al. (2010, 2012) developed a lithosphere-scale 3D structural model for the federal state of Brandenburg (Fig. 1) by integrating more detailed information on the geometries of Permo-Carboniferous to Quaternary units as published in the Geological Atlas of Brandenburg (Stackebrandt and Manhenke 2002). Additionally available for the Berlin area is a 3D hydrostratigraphical model of the main Cenozoic aquifer systems based on 37 hydrogeological cross-sections as correlated with information from 35 boreholes (Jaroch 2006).

The new lithosphere-scale 3D structural model of Berlin (Fig. 2) integrates information on the geometries of geological units derived from three main sources: (1) the lithosphere-scale 3D geological model of Brandenburg with a horizontal resolution of 1 km (Noack et al. 2010, 2012), (2) the 3D hydrostratigraphical model of Cenozoic units in Berlin with a horizontal resolution of 0.5 km (Jaroch 2006), and (3) new stratigraphic and lithological data from four deep boreholes located in or close to the city of Berlin (see Fig. 2 for their locations). As consequence, the structural model is fully consistent with both the regional geological context and with local observations.

Two boreholes have been made available for this study providing information about the real temperatures at greater depths: the temperature log of the well *Velten* with a maximum depth of 1,558 m and the log at *Wartenberg* with a maximum depth of 1,810 m below sea level (Fig. 2). We use this database for the final validation of the 3D thermal models.

The identification of representative thermal and hydraulic properties for the different formations to be used in geothermal modelling is a difficult task, as discussed by Norden et al. (2012), for

example. In this regard, the present study benefits significantly from previous work in the NEGB. For instance, radiogenic-heat-production values have been determined for the main geological units of the sediments and crust based on laboratory measurements, well log and chemical analyses (Norden and Förster 2006; Norden et al. 2008, 2012). A similarly comprehensive database of thermal conductivities measured on drill core samples is available (Fuchs and Förster 2010; Norden and Förster 2006; Norden et al. 2008). However, we additionally use temperature logs available for the boreholes *Velten* and *Wartenberg* to derive rock thermal conductivity from observed temperature gradients. For this purpose, we followed an approach for the inverse calculation of bulk thermal conductivity from the local heat-flow density and the log-derived interval temperature gradient (Blackwell and Steele 1989). The applicability of this procedure in the NEGB was already demonstrated by Fuchs and Förster (2010). As the resulting thermal-conductivity values reflect real *in-situ* conditions, no further temperature or pressure corrections are necessary. For the present study, the interval temperature gradients are computed from high-precision temperature measurements (logged under thermal equilibrium conditions; LIAG 2009). The interval heat flow values, in turn, were computed based on an average surface heat-flow density of 77 mW/m² that represents a mean value estimated for the NEGB where values range between 68 and 91 mW/m² (Norden et al. 2008).

3 Geological model

For compiling, visualising and interpolating 3D information on the structural configuration of the Berlin subsurface we use the commercial software package *Petrel* (©Schlumberger). Subsequently, the final integration of defined geological bodies into a consistent 3D model is performed with *GMS* (*GeoModelling System* developed at GFZ; Bayer et al. 1997) that allows solving numerical problems based on the finite element method. The new model is 53 km wide in east-west direction and 43.5 km in north-south direction (Fig. 2). It differentiates 21 geological units with different lithological properties so that the vertical grid spacing of the 3D model is given by the number of layers and their individual thickness variations (Fig. 2). The base of the model reaches down to the Lithosphere-Asthenosphere Boundary (LAB) at almost 130 km depth (Tab. 1). Horizontally, the 3D structure of each geological layer is defined at 107x88 grid nodes corresponding to a grid spacing of 0.5 km.

3.1 Geological units

Direct information on the litho-stratigraphic subsurface structure is provided by the four boreholes, especially by the *Berlin* and *Oranienburg* wells both penetrating the complete Mesozoic and

Cenozoic succession down to the unit of Permo-Carboniferous volcanics (Fig. 2). The drilled stratigraphic succession reveals lithological properties (Tab. 1) that are quite typical for large parts of the NEGB (Bayer et al. 1997; Hoth et al. 1993).

The Tertiary and Quaternary units represent unconsolidated sand-rich clastics, an exception being the Rupelian Clay unit that is almost exclusively made of unconsolidated clay and represents an important regional aquitard between the shallow freshwater aquifers (Aquifers 1-4) and the deeper saline groundwater aquifers.

The Mesozoic units mainly contain fine-grained clastic rocks (silt- and claystones) and carbonates. Only some formations are made of larger amounts of sandstone, the thickest among them being the Middle Buntsandstein that thus provides favourable conditions for groundwater flow.

Rocks of the Permian time are represented by three units (Fig. 2): on top, the Zechstein unit consists predominantly of rock salt; this salt layer is underlain by the Sedimentary Rotliegend unit, another sandstone-rich, water bearing reservoir formation; the lowermost unit is composed of rhyolites and andesites that partly document volcanic activity of latest Carboniferous times (Benek et al. 1996).

Underlying the Permo-Carboniferous volcanics, the model comprises a layer of strongly consolidated Pre-Permian clastics as found in large parts of the NEGB (Maystrenko and Scheck-Wenderoth 2013). Finally, the sub-sedimentary domains of the lithosphere are represented by an upper crust of granitic to granodioritic composition, a gabbroic lower crust, and a lithospheric mantle assumed to consist of peridotites.

3.2 Geometries of units

In the following, some of the structural characteristics of the new 3D structural model are described in more detail as they are essential for the assessment and understanding of the subsurface thermal field (Fig. 3, 4). Additionally, Table 1 provides an overview on the depth and thickness ranges of all modelled units.

Located in the North German Lowlands, the city of Berlin is characterised by a flat topography with elevations in the range of 10-100 m (Fig. 3a). The city encloses a large NW-SE striking topographic low that gives space to the Spree river system.

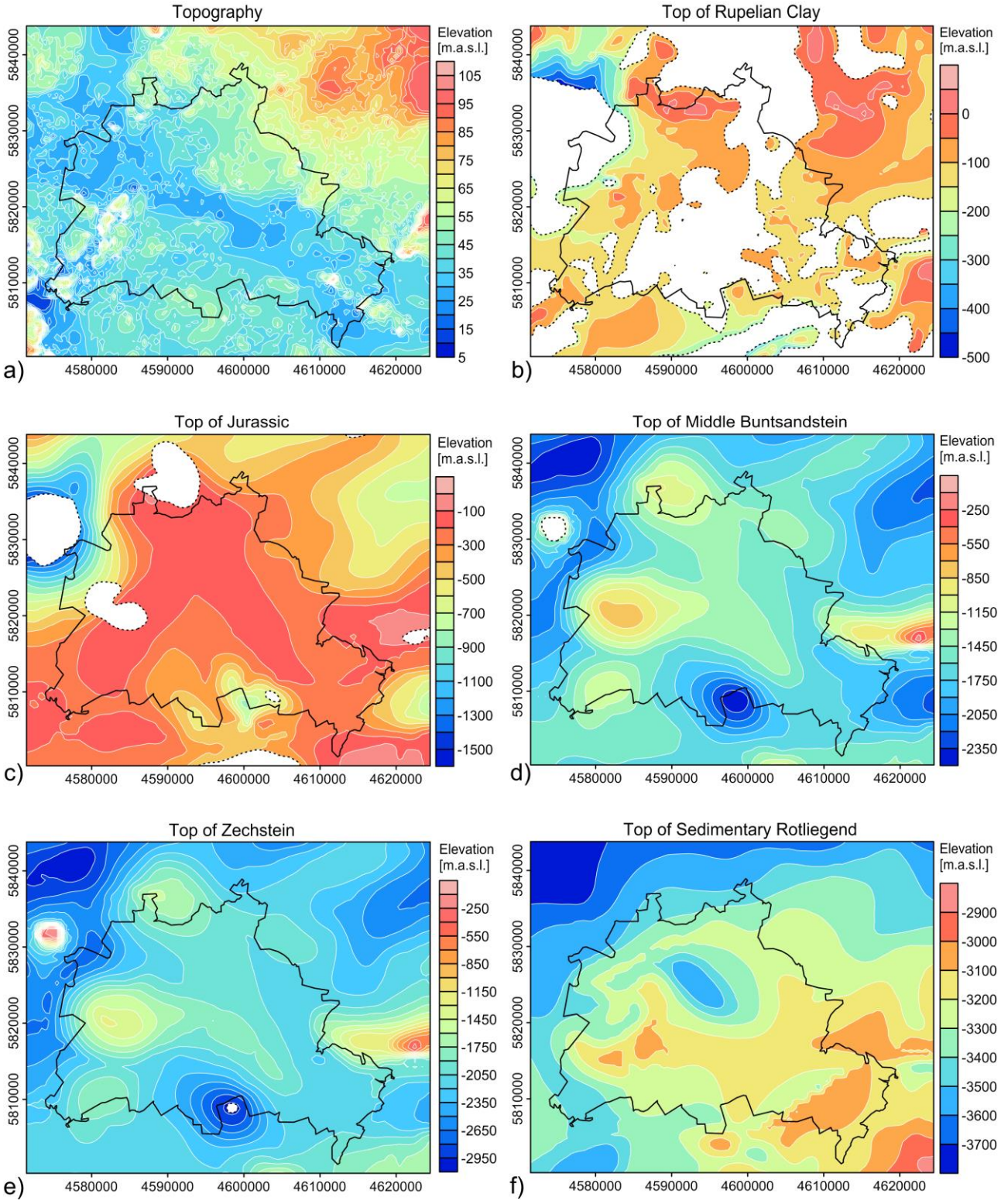

Fig 3 Depth distribution of selected interfaces of the 3D geological model. Areas in which the respective unit is absent are shown in white and surrounded by stippled lines; (a) topography; (b) top of Rupelian Clay; (c) top of Jurassic; (d) top of the Middle Buntsandstein; (e) top of Zechstein; (f) top of Sedimentary Rotliegend; abbreviations: m.a.s.l. - metres above sea level; coordinates [m] in Gauß-Krüger DHDN Zone 4

The base of the freshwater aquifer system of Berlin (i.e. the base of Aquifer 4) is widely formed by the top of the Rupelian Clay unit located at depths of mostly 0-250 m below sea-level (Fig. 3b). This unit reaches maximum thicknesses of some 380 m northwest of Berlin. As already stated, the Rupelian Clay aquitard provides the major natural hydrogeologic boundary separating the

groundwater aquifer used for the internal supply of drinking water in the city from the brackish-to-saline Mesozoic aquifers below. The large gaps revealed by the thickness map of the unit (Fig. 4a) document existing hydraulic connections between the supra- and sub-aquifer systems (hydrogeological windows) that correlate either with major Quaternary glacial erosional channels cutting through the Rupelian aquitard or non-depositional unconformities.

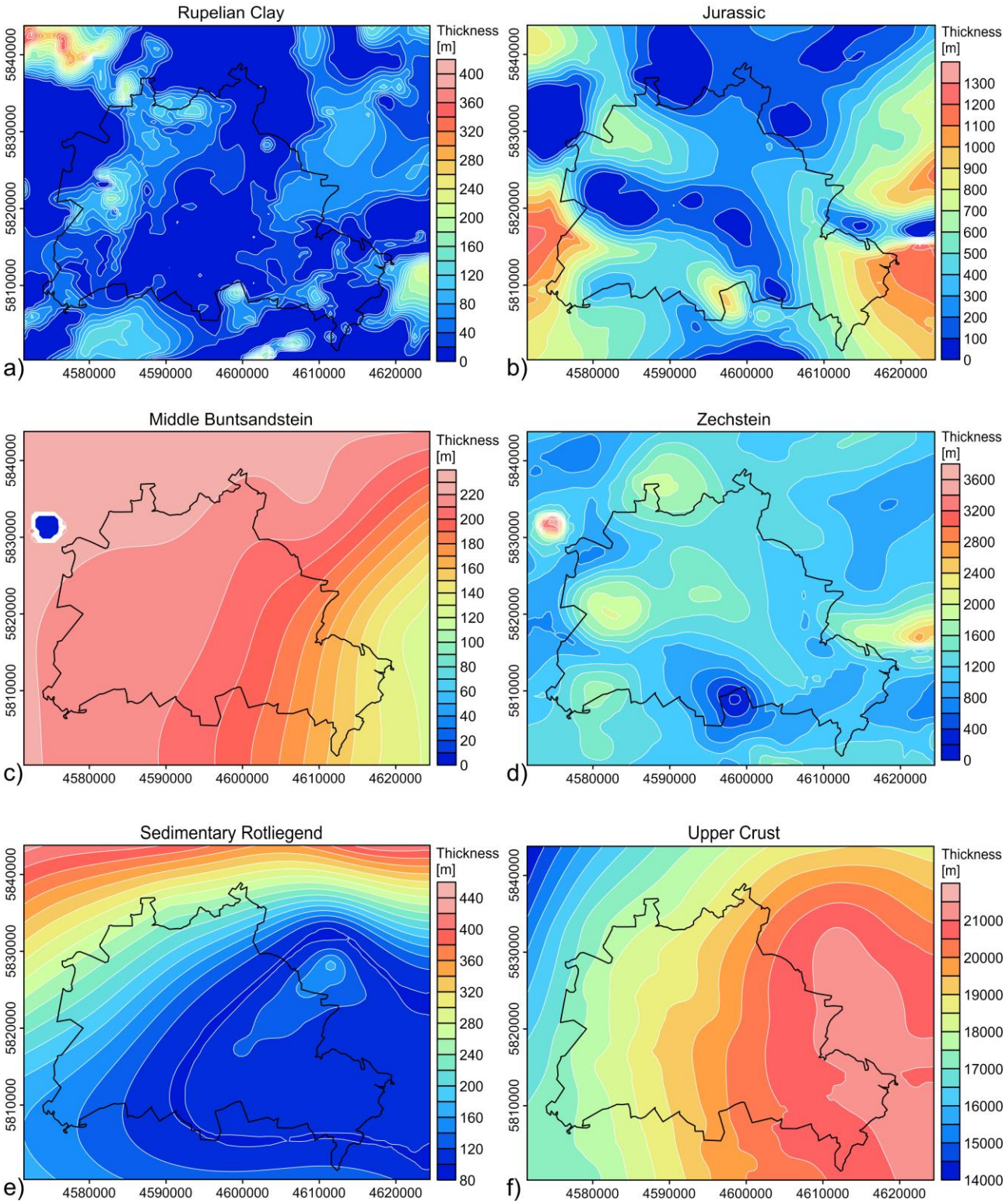

Fig 4 Thickness maps for selected units of the 3D geological model (coordinates [m] in Gauß-Krüger DHDN Zone 4); (a) Rupelian Clay; (b) Jurassic; (c) Middle Buntsandstein; (d) Zechstein; (e) Sedimentary Rotliegend; (f) Upper Crust

The tops of the Jurassic unit (Fig. 3c), the Middle Buntsandstein (Fig. 3d) and the Zechstein salt layer (Fig. 3e) show remarkably similar geometries with agreeing spatial distributions of spatial highs and lows. For example, in the southern parts of Berlin, the top of the Zechstein layer reaches maximum depths of more than 2900 m below sea-level and the tops of the Jurassic and Middle Buntsandstein show topographic lows there as well. Similarly, the most prominent highs of the Zechstein are either retraced by the two Mesozoic tops or these units are missing in such areas (Fig. 4b, c). In contrast to the complex geometry of the top of the Zechstein salt, its base (the top of the Sedimentary Rotliegend unit; Fig. 3f) forms a relatively flat interface, gently deepening towards the northwest, which is towards the centre of the NEGB.

Table 1 Units of the 3D lithosphere-scale geological model of Berlin

Geological unit		Prevailing lithology	Elevation of top [m.a.s.l.]		Thickness variation [m]
			min	max	
Pleistocene to Holocene	Aquifer1	Sand, silt and clay	18	100	0-79
	Aquifer2	Sand, silt and clay	-11	60	0-115
	Aquifer3	Sand, silt and clay	-95	30	0-489
Paleocene to Pliocene	Aquifer4	Sand, silt and clay	-491	43	0-487
	Rupelian Clay	Clay	-546	23	0-384
	Pre-Rupelian	Sand, silt and clay	-546	-25	0-1,100
Creta-ceous	Upper	Limestone with marl	-1,552	-25	0-623
	Lower	Marl with claystone	-655	-150	0-68
	Jurassic	Claystone with silt- and sandstone	-1,537	-25	0-1,326
Triassic	Keuper	Claystone with marl and gypsum	-1,950	-64	0-649
	Muschelkalk	Limestone with marl	-2,004	-15	0-298
	Upper	Silt- and sandstone, rock salt and	-2290	-50	0-217
	Middle	Sandstone with silt- and claystone	-2470	-159	0-221
	Lower	Silt- and claystone	-2691	-163	0-355
Permian	Zechstein	Rock salt with gypsum and	-3,045	-149	171-3,442
	Sedimentary Rotliegend	Claystone with silt- and sandstone	-3,785	-2,890	92-426
Permo-Carboniferous		Rhyolite and andesite	-4,209	-2,900	59-1,034
Pre-Permian		Strongly compacted clastics	-4,750	-3,341	2,148-5,368
Upper crust		Granite and Diorite	-9,687	-5,502	14,055-21,323
Lower crust		Gabbro	-28,331	-23,598	3,770-8,458
Lithospheric mantle		Peridotite	-32,209	-31,858	91,764-97,543
Asthenosphere			-129,604	-123,623	

The geometries of the Mesozoic units reflect much of the halokinetic activity of the underlying Permian Zechstein salt, which was locally mobilised during different times of the tectonic history of the Central European Basin System. In addition, the thickness of the Middle Buntsandstein shows a substantial east-to-west increase across the Berlin area (120-240 m; Fig. 4c), except for an area northwest of the city where the unit is not present above a large Zechstein diapir structure. Such a

homogeneous thickness distribution only pierced by the northwestern salt diapir (Fig. 2) is also shown by the Lower and Upper Buntsandstein and the Muschelkalk.

Similarly, the Jurassic sediments show zero thicknesses above the most prominent Zechstein highs (Fig. 4b, d). However, the thickness distribution of the Jurassic sediments is more complex with strong thickness increases in the direct vicinity of Zechstein structural holes. This configuration reflects the development of rim synclines typical for the NEGB, i.e. depocentres surrounding the salt domes and diapirs that were filled by the Jurassic sediments while the salt below was moving into the domes (e.g. Scheck et al. 2003). Similar present-day thickness distributions, related to non-deposition above active salt structures and maximum sediment accumulation around them, are shown by the units of the Keuper and the Pre-Rupelian Clay Tertiary. The preserved thicknesses of Cretaceous sediments do not reveal such a clear relationship to salt activity as they are absent across most of the Berlin area with localised thickness maxima in its northeastern parts.

In the sub-salt parts of the model, the thickness of the Sedimentary Rotliegend unit (the deeper potential geothermal target horizon) gradually increases from about 100 m in the south to more than 400 m in the northern Berlin area (Fig. 4e). This thickness trend appears largely unaffected by the thickness variation of the underlying Permo-Carboniferous Volcanics: the volcanic unit forms a circular-shaped structure of up to ~1,000 m thickness at the northern border of the city from where thins out to less than 100 m.

The thickness of Pre-Permian sediments increases from about 2,200 m in the southeast to more than 5,000 m in the northwest. The reverse trend is shown by the upper crust which shows an increase in thickness from about 14 km in the west to more than 20 km under the eastern parts of Berlin (Fig. 4f). The crust-mantle boundary (Moho) is located at depths of about 32 km, while the LAB reaches as deep as 124-130 km (Tab. 1).

4 Thermal modelling approaches

To predict the temperature distribution of the deep subsurface, we perform two different types of heat-transport simulations: first, we calculate the steady-state conductive thermal field on a full lithosphere scale and, second, we consider the dynamic effects of groundwater by simulating 3D coupled fluid and heat transport within the sedimentary sequence. Both approaches hold certain advantages and limitations as will be discussed in Section 5.

4.1 Conductive thermal field (Model A)

For the purely conductive temperature calculations, we assume that heat is transported predominantly by conduction throughout the Earth's lithosphere. The mathematical formulation of the relevant equation reads as:

$$(\rho c)^{(b)} \frac{\partial T}{\partial t} = -\nabla * (\lambda^{(b)} \nabla T) + S \quad (1)$$

A list of all parameter used may be found in Table 3.

Table 3 Nomenclature of all parameters used in the numerical simulations

Roman		
c^0	solid or fluid heat capacity	[kJ kg^{-1} K^{-1}]
D	thermodispersivity tensor	[m^2 s^{-1}]
g	gravity force	[m s^{-2}]
I	unit tensor	[-]
k	permeability tensor of the porous medium	[m^2]
p	pressure	[Pa]
S	rock radiogenic heat production	[μW m^{-3}]
t	time	[s]
T	temperature	[°C or K]
Q^0	fluid and solid mass source-sink term	[kg m^{-3}s^{-1}]
q	Darcy velocity	[m s^{-1}]
Greek		
ϵ	porosity, void space fraction	[-]
λ^0	fluid , solid or bulk thermal conductivity	[W m^{-1} K^{-1}]
ρ^0	fluid or solid density	[kg m^{-3}]
μ	fluid dynamic viscosity	[Pa s]
∇	Nabla operator	[m^{-1}]
Superscripts		
b	bulk (liquid + solid)	
l	liquid phase	
s	solid phase	

Under the assumption of thermal equilibrium (i.e. steady state), the first term on the left hand side of Equation 1 can be neglected (i.e. $\frac{\partial T}{\partial t} = 0$). Accordingly, Equation 1 takes the simplified form of:

$$\nabla * (\lambda^{(b)} \nabla T) = S \quad (2)$$

From Equation 2 it follows that calculated temperatures are sensitive only to the radiogenic heat production (*S*), the bulk thermal conductivity ($\lambda^{(b)}$), and the choice of boundary conditions. We numerically solve the three-dimensional equation of heat conduction by using a 3D Finite Element Method implemented in the software package *GMS* (Bayer et al. 1997).

To calculate the 3D conductive thermal field, each unit of the 3D geological model is assigned a constant value for the radiogenic heat production and the bulk (solid and fluid) thermal conductivity (Tab. 2). Since direct information on the thermal properties of rocks in the subsurface of Berlin is still sparse, e.g. core samples on which laboratory measurements could be performed, we partly revert to measured data from the same stratigraphic units in other parts of the NEGB (Norden and Förster 2006; Norden et al. 2008).

While the lateral boundary conditions of the model are considered to be closed, a constant temperature of T=8°C at the Earth's topographic surface (Fig. 3a) has been defined as upper boundary condition. This temperature corresponds to the average annual surface temperature in those parts of Berlin where temperatures are least influenced by urban development (data for 2010; Henning and Limberg 2012). For the definition of the lower boundary condition, we use the same approach as Noack et al. (2012): we assume the LAB to represent the depth where the mantle adiabat cuts the geotherm thus forming an isotherm of T=1,300°C (i.e. corresponding to the solidus of mantle peridotite). Accordingly, the lower boundary condition for the purely conductive thermal modelling corresponds to a temperature of 1,300°C at the LAB. The base of the lithosphere beneath Berlin (Tab. 1) is derived from a 3D structural model of the Central European Basin System, which is consistent with seismological experiments and constrained by 3D gravity modelling (Maystrenko and Scheck-Wenderoth 2013). This LAB has been shown to be consistent with the observed thermal field in the Brandenburg region (Noack et al. 2012).

4.2 Coupled conductive-convective thermal field (Model B)

In order to consider additional heat transport processes by moving groundwater, 3D numerical simulations of coupled heat and fluid flow are carried out by means of the commercial software FEFLOW® (Diersch 2009). This software package enables to simulate saturated and unsaturated flow in complex porous geological formations taking into account both linear advective and nonlinear buoyant heat transport mechanisms. The former topography-, tectonically, or over-pressure driven flow arises from existing lateral pressure gradients that represent the major source of regional groundwater flow in geologically compartmentalised aquifer systems. The latter quantifies the amount of groundwater buoyant flow self-sustained by internal changes in the fluid density due to thermal expansion of the fluid (thermal buoyancy term) and variations in its compressibility (pressure buoyancy term). Additional effects related to buoyant flow induced by gradients in the solutal fluid compositions are not taken into account in the present study.

The mathematical formulation for the coupled fluid and heat transport problem is defined by three nonlinear and coupled Partial Differential Equations (PDEs) leading to a classical initial and boundary value problem. Equations 3-5 detail the corresponding PDE system for the problem at

hand (e.g. Bear 1979; Nield and Bejan 2006). A list of all parameters and their units is given in Table 3.

$$\frac{\partial[\epsilon\rho^{(l)}+(1-\epsilon)\rho^{(s)}]}{\partial t} + \nabla * (\epsilon\rho^{(l)}\mathbf{q}) = \epsilon Q^{(l)} + (1-\epsilon)Q^{(s)} \quad (3)$$

$$\frac{\partial[\epsilon\rho^{(l)}c^{(l)}+(1-\epsilon)\rho^{(s)}c_p^{(s)}]T}{\partial t} = -\nabla * (\epsilon\rho^{(l)}c^{(l)}\mathbf{q} * T) - \nabla * \{[(\lambda^{(b)}\mathbf{I}) + (\rho^{(l)}c^{(l)})\mathbf{D}] * \nabla T\} + (1-\epsilon)S \quad (4)$$

$$\mathbf{q} = -\frac{k}{\epsilon\mu}(\nabla p - \rho^{(l)}\mathbf{g}) \quad (5)$$

Equation 3 represents the mass balance, Equation 4 the internal energy balance for the system. These two sets of equations are then coupled by the linear momentum conservation equation (Equation 5), which has been derived under the assumptions provided by Darcy's law. Nonlinearities arise from considering thermal and pressure effects on the fluid density. To close the PDE, an additional Equation Of State (EOS) for the fluid density is therefore required by which to represent the fundamental thermodynamic relations between the fluid-state variables (p and T) and the fluid density ($\square^{(l)} = \square^{(l)}$ (p,T); e.g. Blöcher et al. 2010).

To investigate the effects of advective and buoyant flow on the thermal field, the numerical simulations are carried out by considering the sedimentary succession as represented by the lithosphere-scale geological model described in Section 3. However, given the nonlinearity of the PDE, additional efforts have been required to set up a proper computational mesh that correctly integrates all geometric information while meeting numerical quality criteria. The horizontal resolution of the input geological model (500 x 500) m has been increased to a (200 x 200) m scale. In order to guarantee a good vertical-to-horizontal element shape ratio, all layers have been vertically refined. As a result, all layers are made up by at least two finite element sequences and no element has a vertical extent greater than the imposed horizontal resolution. The final mesh thus consists of 4,057,680 triangle shaped prismatic elements arranged in 55 computational layers.

The system of PDEs (Eq. 3-5) with a proper EOS for the fluid density leads to an initial and boundary differential problem that requires the specification of proper fluid and thermal boundary and initial conditions. For the upper thermal boundary condition, a constant temperature of T=8°C has been fixed along the topographic elevation of Berlin, which allows direct comparison with the purely conductive Model A. To minimise the number of finite elements and thus the computational effort for the coupled simulations, the lithosphere-scale 3D structural model was cut at a constant depth of -6,000 m. By using this maximum depth, the entire sedimentary sequence is considered plus an additional impervious basement. Accordingly, the lower thermal boundary condition has been set as the temperature distribution at a depth of -6,000 m extracted from the lithosphere-scale purely conductive Model A (Fig. 6a). Although being smaller in extent, the coupled Model B still

covers depths of interest for geothermal usage. Finally, the lateral boundaries are considered closed to heat flow.

The initial conditions for the coupled simulations are specified by the temperature distribution of Model A and the pressure distribution as obtained from steady-state simulations of flow. The upper flow boundary condition, i.e. the groundwater level, is approximated by setting the hydraulic head equal to the topographic elevation in the study area (Fig. 3a). All other boundaries are considered as no-flow boundaries.

Because of the highly nonlinear coupled problem we are solving for and the complex geometry of the simulation domain, which both prevent obtaining stable steady-state solutions, transient simulations are run. By letting the coupled simulations run for 200,000 years of computational time (being no attempt to reconstruct the past evolution), the system finally reaches a stable (quasi steady-state) p-T configuration. The final results of these simulations thus represent a numerical proxy of the present-day thermal field.

Table 2 Properties of the geological units as used for the thermal calculations

Geological unit	Bulk thermal conductivity $\lambda^{(b)}$ [$Wm^{-1}K^{-1}$]	Radiogenic heat production S [μWm^{-3}]	Rock heat capacity $c^{(s)}$ [$kJkg^{-1}K^{-1}$]	Effective porosity ϵ [-]	Permeability k [mD]
Aquifer1	3.5[x]	0.9[#]	2.16[§]	0.311[§]	10
Aquifer2	3.5[x]	0.9[#]	2.16[§]	0.311[§]	10
Aquifer3	3.5[x]	0.9[#]	2.16[§]	0.311[§]	10
Aquifer4	3.5[x]	1.0[#]	2.16[§]	0.311[§]	10
Rupelian clay	1.88[x]	1.3[#]	2.36[§]	0.194[§]	0.1
Pre-Rupelian clay	3.1[x]	1.3[#]	2.26[§]	0.255[§]	10
Upper Cretaceous	2.82[x]	0.6[#]	2.29[§]	0.110[§]	50
Lower Cretaceous	2.36[x]	1.5[#]	2.29[§]	0.110[§]	50
Jurassic	2.71°	1.5[#]	2.25[§]	0.189[§]	50
Keuper	2.35°	1.6[#]	2.32[§]	0.128[§]	10
Muschelkalk	2.3[x]	1.0[#]	2.25[§]	Section 4.2	Section 4.2
Upper Buntsandstein	3.0[x]	1.8[#]	2.19[§]	0.025	0.67
Middle Buntsandstein	2.0[x]	1.8[#]	2.39[§]	0.135	60.76
Lower Buntsandstein	1.84[x]	1.8[#]	2.39[§]	0.049	0.13
Zechstein	4.5[+]	0.4[#]	1.94[§]	0.005	0.0001
Sedimentary Rotliegend	3.0[x]	1.4[#]	2.18[§]	0.078	5.26
Permo-Carboniferous	2.5[#]	2.9[§]	2.60[§]	0.032	0.09
Pre-Permian	2.2[§]	2.8[§]	not used	not used	not used
Upper Crust	3.0[+]	2.3[+]	not used	not used	not used
Lower Crust	2.4[+]	0.4[+]	not used	not used	not used
Lithospheric Mantle	4.1[+]	0.01[+]	not used	not used	not used

Parameter values were derived from (+) Norden et al. (2008), (°) Fuchs and Förster (2010), (#) Norden and Förster (2006), (§) Norden et al. (2012), and (x) available temperature logs. Porosity values for the Upper Buntsandstein and underlying layers as well as all permeability values correspond to laboratory measurements of drill core material from the available four boreholes.

As for the purely conductive Model A, each geological layer has been populated by constant fluid and rock properties that are listed in Table 2. Areas of zero thickness of a layer are automatically assigned a minimum thickness of 0.1 m by the software to assure continuum conditions for the solution of the equations in the finite element model. In order to integrate into the numerical model existing discontinuities (geological holes) characterizing the Rupelian Clay unit, the geometries of these hydrogeologic windows have been forced onto the model by means of a constrained triangulation around their boundaries. A GIS-based approach has then been followed to set the correct parameterisation in these subdomains (for more details see Kaiser et al. 2011). For the simulations, holes in the Rupelian succession share the same set of properties with the overlying upper Tertiary aquifer (Aquifer 4).

Special reference needs to be made for the fluid parameterisation adopted for the Middle Triassic Muschelkalk layer. Previous studies have considered this layer to act as an impervious stratum (Kaiser et al. 2011; Magri et al. 2008). However, more recent studies have contributed towards a better assessment of its productivity for geothermal resources (Philipp et al. 2011). Additional studies performed on the Muschelkalk formation in the north-eastern Netherlands (Pöppelreiter et al. 2005) have delineated a (tri)partition of the sedimentary sequence into porous Lower and Upper Muschelkalk carbonates, separated by a tight Middle Muschelkalk succession. Following these suggestions, the uniform Muschelkalk layer of the lithosphere-scale 3D structural model has been equally subdivided into a sequence of three minor units representing the Lower, Middle, and Upper Muschelkalk. While sharing the same thicknesses and thermal rock properties, the three layers have been differentiated in terms of their flow related properties (i.e. porosity and permeability). Following Pöppelreiter et al. (2005), an average porosity of $\epsilon = 0.12$ and a permeability of $k = 0.06$ mD have been set for the Lower Muschelkalk, while $\epsilon = 0.15$ and $k = 1$ mD have been assigned to the Upper Muschelkalk. The Middle Muschelkalk unit has been considered to be tight.

5 Predicted temperatures

For a better comparison of the results and underlying processes, Model A and Model B are designed to be consistent in terms of boundary conditions, radiogenic heat production, and thermal conductivity. Thus, their set-ups differ only in the additional parameters (porosity, permeability,

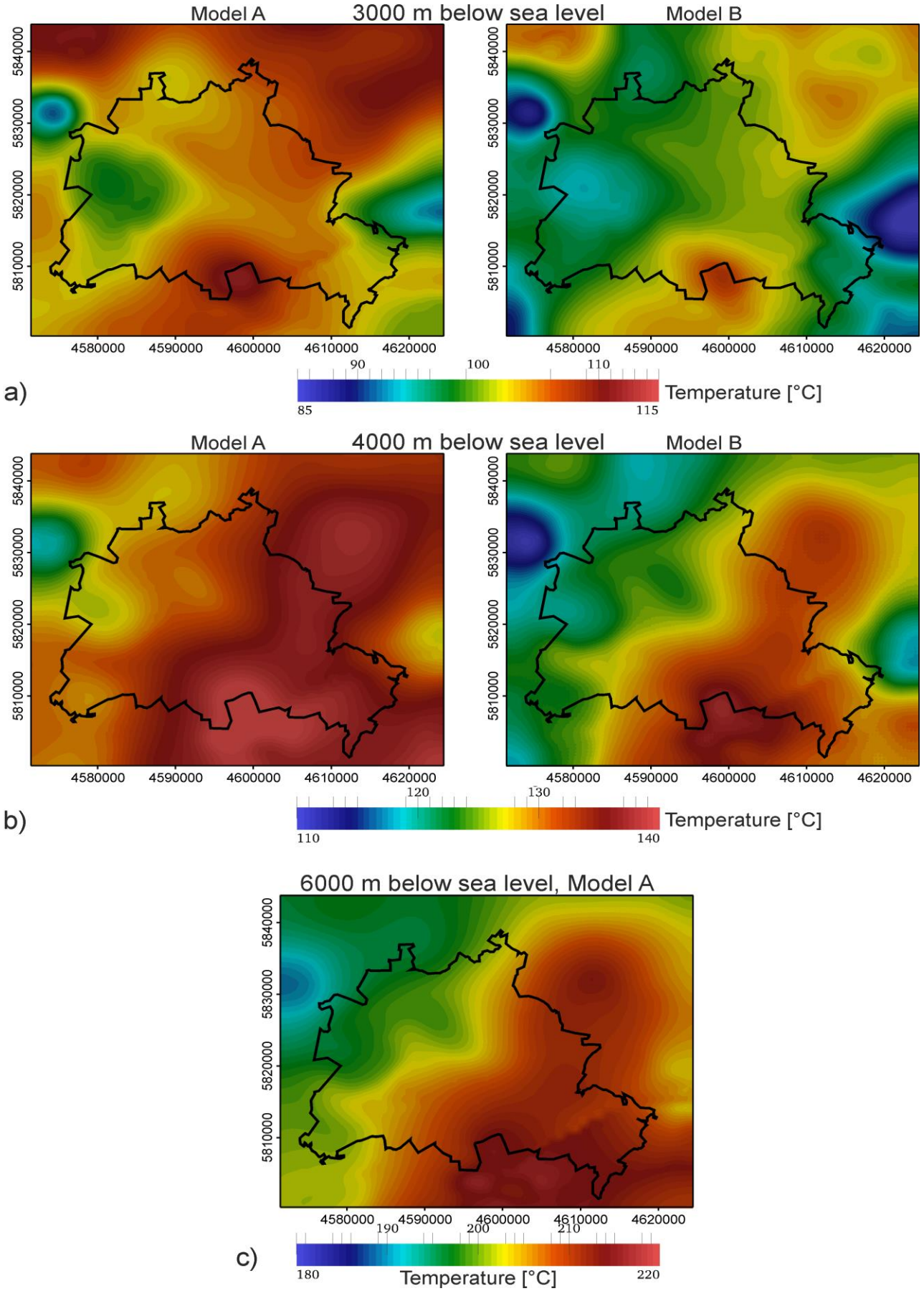

Fig 5 Temperature distribution predicted by the purely conductive Model A (left) and the coupled Model B (right) for selected constant depth levels (below sea level); (a) temperatures at 3,000 m depth; (b) temperatures at 4,000 m depth; (c) temperatures at 6,000 m depth used as the lower thermal boundary condition for the coupled thermal simulations; all coordinates in Gauß-Krüger DHDN Zone 4

heat capacity) and physical laws implemented in the coupled fluid and heat transport simulations of Model B.

Figures 5 and 6 illustrate temperature maps as extracted from the two model realisations for different constant depth levels. The temperatures at 6 km depth (Fig. 5c), calculated by Model A and taken as the lower boundary condition for Model B, show a clear northwest to southeast trend with temperatures decreasing from more than 215°C to less than 190°C. The main explanation for this trend lies in the Upper Crust, which by its volume and composition is the most important source of radiogenic heat (Tab. 2) and shows decreasing thicknesses from the southeast to the northwest (Fig. 4f). Furthermore, a circular-shaped temperature low northeast of Berlin is positioned beneath the maximum thickness of the Zechstein salt layer (Fig. 4d). The Zechstein rocks are characterised by the largest bulk thermal conductivity (Tab. 2) and thus most effectively transport heat out of the sedimentary basin.

This process leads to lateral temperature differences underneath the Zechstein correlating inversely with the thickness distribution of the unit. Also at 4 km depth, which is beneath the salt (Tab. 1), the lowest temperatures are predicted for the area northwest of Berlin where the Upper Crust is thinnest and the salt diapir induces the modelled negative thermal anomaly (Fig. 5b). The thermal pattern at 3 km depth (Fig. 5a), which still is located largely below the salt, shows even more correlations with the thickness distribution of the salt layer. Four distinct areas of low temperatures are visible, which can directly be correlated with four salt thickness maxima (Fig. 4d). In contrast, where the Zechstein salt thins out or is even missing, like at the southern border of Berlin, local temperature highs are predicted for 3 km depth. These hot areas are caused by the relatively small thermal conductivity and related thermal blanketing effect of overlying sediments (Tab. 2).

For areas above the salt, the efficiency of the Zechstein salt layer in transporting heat upwards leads to the opposite thermal pattern, documented by predicted temperatures at depths of 1 km and 2 km that are higher where the salt is thick (Fig. 6a, c). This supra-salt conductivity-induced warming is also reflected by the lateral variations of the average geothermal gradient between the top of the Zechstein and the base of the Rupelian Clay unit (Fig. 7a). The vertically average geothermal gradient varies between more than 43°C/km in areas above salt domes and less than 35°C/km away from these structures.

Due to the large effect of the high thermal conductivity of the Zechstein salt layer, the predicted overall pattern of negative and positive thermal anomalies is remarkably similar for Model A and Model B (Fig. 5, 6). However, the temperature distribution becomes more complex and more dissimilar towards shallower depths. A general difference between the two types of models regards the predicted absolute temperatures, which are lower in the case of the coupled Model B (Tab. 4). This difference demonstrates that topography-driven groundwater flow leads to an overall cooling

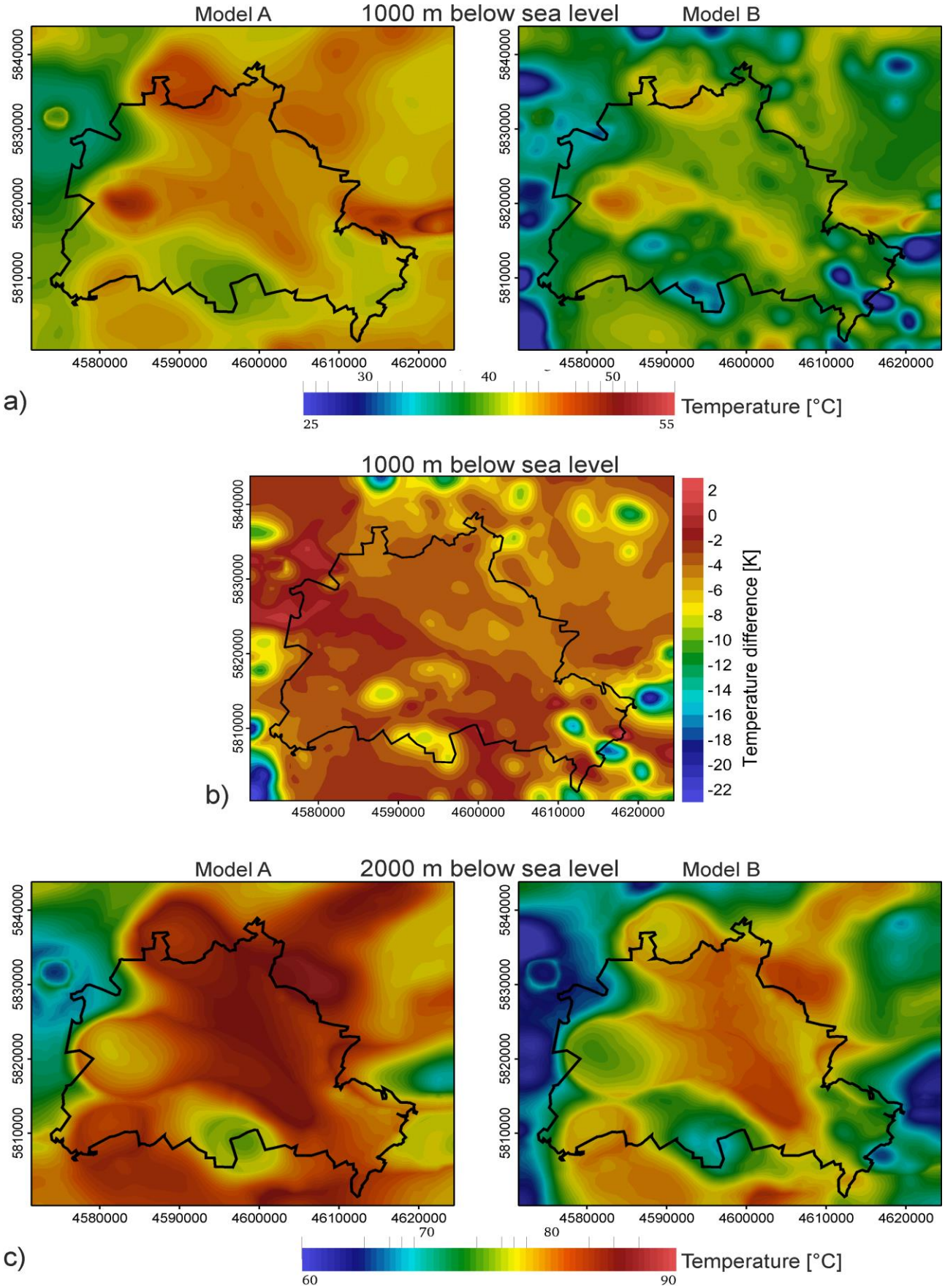

Fig 6 Temperature distribution predicted by the purely conductive Model A (left) and the coupled Model B (right); (a) temperatures at 1,000 m depth (below sea level); (b) difference between temperatures predicted by Model A and Model B for a depth of 1,000 m (below sea level); Model A temperatures were subtracted from Model B temperatures so that negative differences indicate a colder Model B. (c) Temperatures at 2,000 m depth; all coordinates in Gauß-Krüger DHDN Zone 4

of the subsurface. We can also see that at a depth of 1 km, fluid dynamics as considered by Model B causes lateral temperature variations of a smaller scale than observed in the purely conductive Model A (Fig. 6a). Thereby, the differences between the two models at 1 km depth (Fig. 6b) correlate most clearly with the topography of the area (Fig. 3a): Where lateral topography differences and thus the hydraulic potential are high, the temperatures predicted by the coupled Model B are farther shifted from Model A. In addition, larger differences between the models at this depth are located where the Rupelian Clay aquitard (Tab. 2) either reaches larger depths (Fig. 3b) or is missing (hydrogeological windows; Fig. 4a). At these places, the cooling due to entering cold surface water is stronger and propagating faster. In contrast, locations characterised by a thick Rupelian aquitard at shallow depth levels see relatively minor excess cooling.

Although these small-wavelength variations of the thermal field diminish towards greater depth, the overall cooling effect persists even to depths of at least 4 km (Fig. 5b). The modelled temperatures also vary much laterally within the potential geothermal target horizons, the Sedimentary Rotliegend and the Middle Buntsandstein (Fig. 8). At the top of the Sedimentary Rotliegend, a temperature range of 94-125°C is calculated by Model A and a range of 85-139°C by Model B (Fig. 8b). The largest temperatures of the Sedimentary Rotliegend are found north of Berlin where this layer shows its greatest thicknesses (Fig. 4e). However, an important controlling factor for the thermal pattern is the depth position of the unit. The Sedimentary Rotliegend is located about 800 m deeper in the northwest than in the southeast of the study area (Fig. 3f) so that due to the geothermal gradient, there is a general southeast-northwest trend of increasing temperatures. Moreover, the temperature distribution largely reflects the cooling effect of the overlying Zechstein salt inducing lower temperatures where the salt is thicker (Fig. 4d).

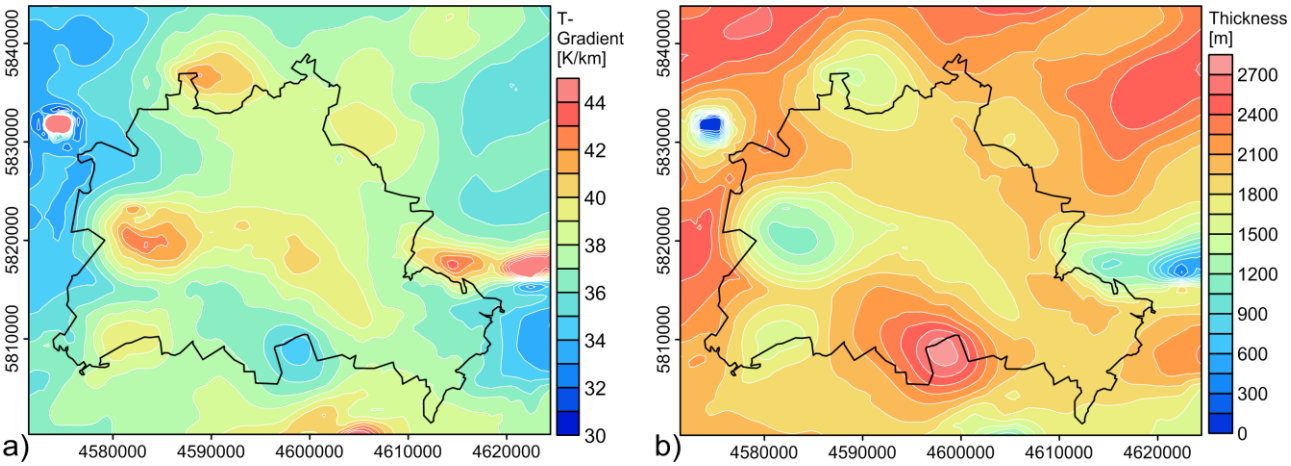

Fig 7 Average geothermal gradient as predicted by the purely conductive Model A (a) and thickness (b) between the base of the Rupelian Clay unit and the top of the Zechstein unit; coordinates in Gauß- Krüger DHDN Zone 4

For the top of the Middle Buntsandstein, temperatures of 17-90°C (Model A) and 15-95°C (Model B) have been calculated (Fig. 8a). Like for the Sedimentary Rotliegend, the large temperature variation along this geological horizon reflects much of its variable depth position (Fig. 3d). Greater

depths correlate with larger temperatures according to the geothermal gradient. Thus, even where located above a dome of thick Zechstein salt transferring much heat into the Buntsandstein, the calculated temperatures are lower because of the shallow position and the thin overlying blanket of younger heat storing sediments.

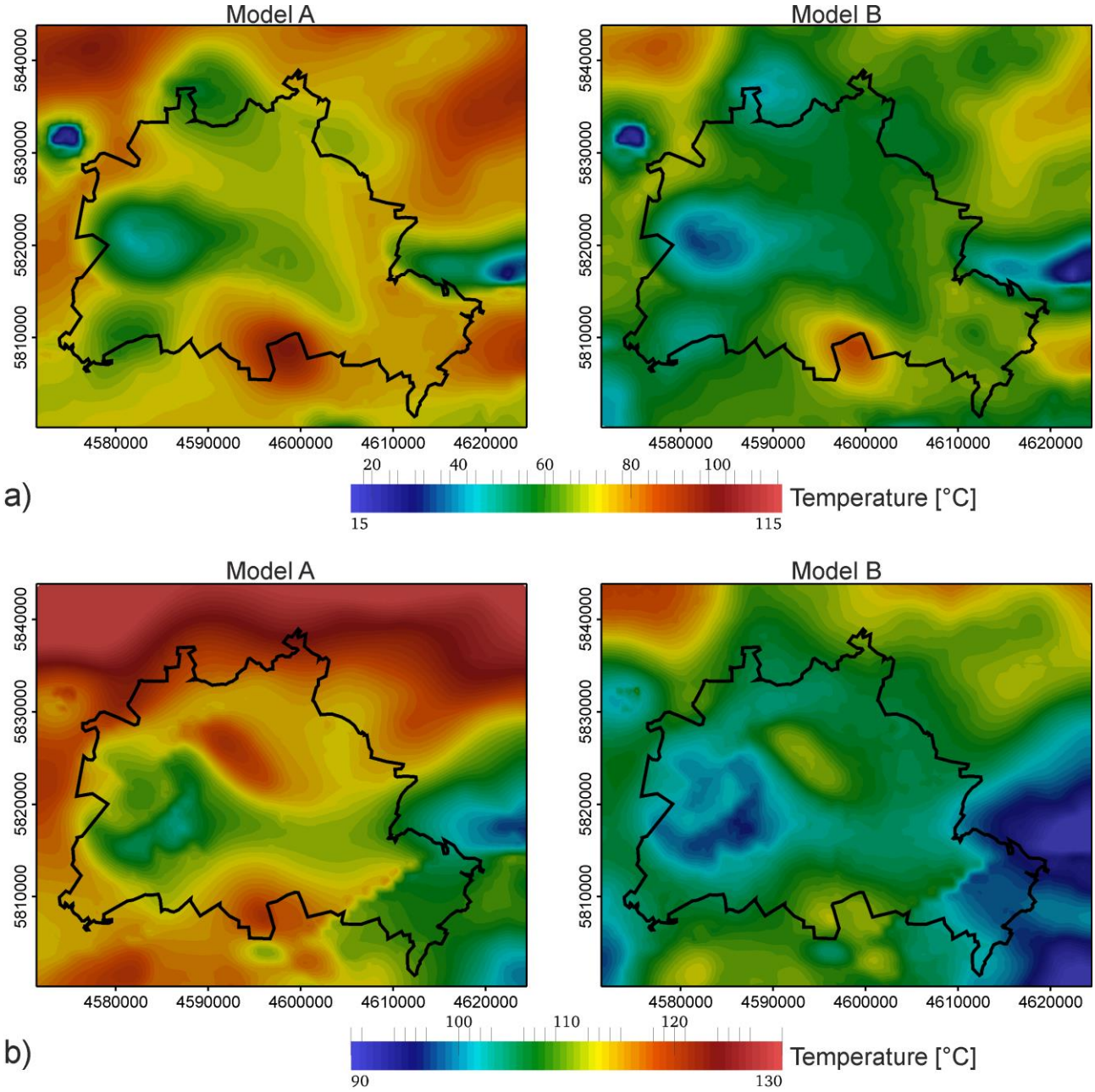

Fig 8 Temperature distribution predicted by Model A (left) and Model B (right) for (a) the top of Middle Buntsandstein and (b) the top of Sedimentary Rotliegend; coordinates are in Gauß- Krüger DHDN Zone 4

6 Discussion

One of the main results of this study is that the subsurface of Berlin shows large lateral temperature variations (Fig. 5, 6). For example, the purely conductive Model A predicts temperatures of 91-112°C for a depth of 3,000 m (below sea level; Tab. 4). Interestingly, the temperatures obtained

for constant depth levels between 2,500 m and 4,000 m by applying 3D geostatistics to observed temperatures from all over Germany (GeotIS; Agemar et al. 2012) fall within the ranges of the purely conductive and the coupled models. However, these geostatistically obtained temperatures differ by less than 10°C across the Berlin area compared to >20°C as implied by Model A and Model B for the same depths. This reflects the difference in resolution, which corresponds to the horizontal distance between single temperature logs for the geostatistical approach, while the geological-physical approach resolves temperature-relevant heterogeneities situated between the wells.

The modelling results show that for the deeper subsurface (e.g. depths of 6 km, Fig. 5c), the relatively high radiogenic heat production and varying thickness of the upper crust (Fig. 4f) plays an important role for the temperature distribution. However, the most significant thermal anomalies predicted by Model A are clearly related to characteristics of the Zechstein salt layer, which is in line with previous studies of the thermal field of the region (e.g. Bayer et al. 1997; Hurtig and Rockel 1992). Thereby, the influence of this layer is twofold. First, its high thermal conductivity leads to differential amounts of heat entering the supra-salt sequence, which is a well-known phenomenon (e.g. Jensen 1990). This may suggest drilling for geothermal energy would be best where the salt is thick (above salt domes and diapirs) and transports more heat upwards. However, where the salt is thin, potential geothermal target horizons of the supra-salt sequence tend to reach greater depths and thus show higher temperatures due to the geothermal gradient.

The intricate role of the Zechstein salt unit is also reflected by the modelled temperature distributions of the two potential target horizons for deep geothermal energy, the Middle Buntsandstein and the Sedimentary Rotliegend (Fig. 8). Given their relative location in the stratigraphic sequence with respect to the salt layer, the chimney effect of the salt has a different impact. Following the geometry of the top of the Zechstein, the Middle Buntsandstein reaches shallower depths and thus colder temperatures above thick salt. Varying burial depths and varying thicknesses of overlying, insulating sediments buffer the temperature-increasing chimney effect. Within the sub-salt Sedimentary Rotliegend, negative thermal anomalies are found in spatial correlation with large thicknesses of the overlying highly conductive salt.

The benefit of the thermal models lies in combining the actual 3D geology with computed temperatures so that certain potential target horizons are attributed with depths and temperatures (Fig. 3, 8). Coevally, economically interesting isotherms – as 70°C relevant for the utilisation of heat and 110°C relevant if electric power production is envisaged – are directly associated to geological units (Fig. 9). Such correlations are important as high drilling costs may set a limit to the maximum depth of a well, the modelled temperatures may imply a minimum drilling depth according to the heat usage aimed for, and the rock type drilled at depth will decide on the

hydrogeological properties controlling the conditions and costs during exploitation. In this regard, Mottaghy et al. (2011) demonstrated the importance of considering heterogeneities in the deep thermal and hydraulic properties for optimally planning a deep injector-producer doublet designed for heating one of the districts of Den Haag.

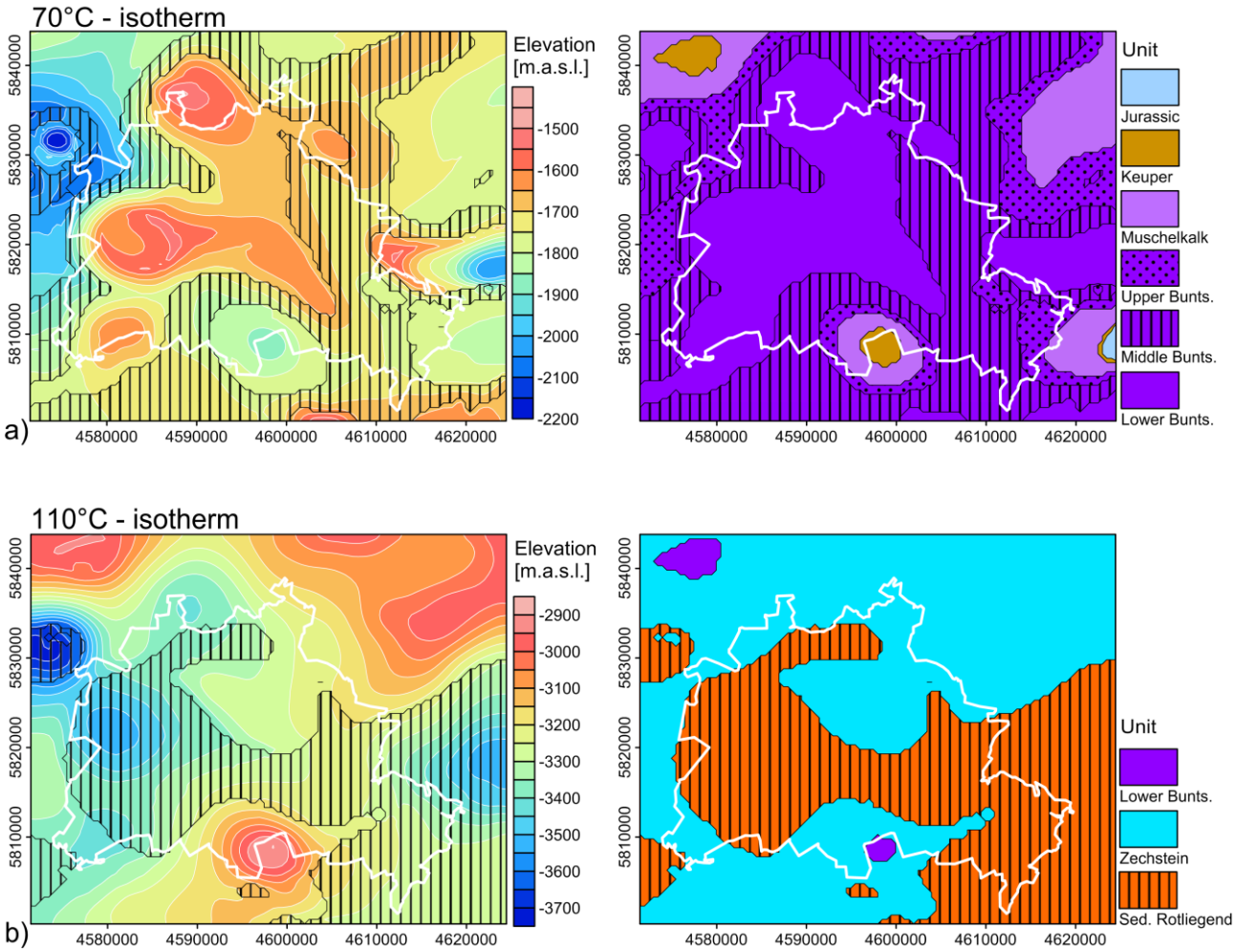

Fig 9 Isotherms predicted by the purely conductive Model A; (a) depth distribution (left) and geological map (right) for the isotherm of 70°C; the hatched areas indicate the distribution of the potential geothermal target of the Middle Buntsandstein; (b) depth distribution (left) and geological map (right) for the isotherm of 110°C; the hatched areas indicate the distribution of the potential geothermal target of the Sedimentary Rotliegend; coordinates in Gauß-Krüger DHDN Zone 4; m.a.s.l. - metres above sea level

6.1 Influence of the geological structure

The 3D geological model is the base for the parameterisation of the thermal models and thus inevitably crucial for the predicted temperatures. Using the 3D structural model of Brandenburg (Noack et al. 2010, 2012) as a base holds important advantages: it already implements information on the configuration of the entire lithosphere for the Berlin area. Thus, the Berlin model is consistent with the main regional trends in present-day geology that also reflect well-known dynamics in the evolution of the entire region (e.g. Maystrenko and Scheck-Wenderoth 2013). For example, recurrent halokinetic phases stepwise increased the number and size of salt domes and

diapirs in the Central European Basin System (Maystrenko et al. 2013). This trend is also revealed by the zero-thickness domains in the supra-salt units of Berlin: such structural holes induced by erosion or non-deposition above thick salt structures increase in number and extent from older units as the Middle Buntsandstein (Fig. 4c) to younger units as the Jurassic (Fig. 4d).

At the same time, the integration of stratigraphic information from four wells (Fig. 2) and from the 3D model of the Cenozoic aquifer system (Jaroch 2006) implies a further refinement of the original Brandenburg model. The largest structural differences between the Brandenburg model and the new Berlin model are related to the post-Permian stratigraphy observed at well *Berlin 01*. At this well, the thickness of the Middle Buntsandstein, for instance, amounts to >200 m (Fig. 2), while the Brandenburg model still predicts complete absence of the entire Buntsandstein sequence there. Thus, the integration of local stratigraphic data means one step towards better characterising this potential target horizon.

While the upper thermal boundary condition for the purely conductive Model A is well constrained by the known topography and surface temperature of the area, the lower boundary condition appears more disputable. An alternative lower boundary condition often used for thermal studies is a defined heat-flow density at the crust-mantle boundary. But the Moho is a chemical, not necessarily a thermal boundary. The LAB of the Berlin model (like the sub-sedimentary crystalline crust) derives from a regional 3D model that is consistent with seismological data and the observed gravity field (Maystrenko and Scheck-Wenderoth 2013). Considering this LAB as the 1,300°C isotherm (mantle solidus), Noack et al. (2012) demonstrates that this thermal boundary and the deep crustal configuration are consistent with a thermal field that reproduces temperature measurements from all over Brandenburg and depths up to 6,820 m. The relevance of this validation becomes evident from an earlier study that showed how sensitive the shallow thermal field of the NEGB is to the depth of the thermal LAB (Cacace et al. 2010). Accordingly, differences in the LAB depth of 20 km may result in temperature differences as high as 30°C at a depth of 5,000 m. As the Berlin model is in line with previous studies on the regional thermal field, we regard the heat budget entering the sediments from the deep crust and lithospheric mantle as well constrained.

6.2 Influence of conductive heat transport

The impact of the highly-conductive Zechstein salt on the thermal field proves the importance of well-constrained thermal conductivities. The thermal conductivities assigned to most of the Mesozoic units are estimated based on temperature-log analysis applied to two wells within the Berlin area (*Velten*, *Wartenberg*; Fig. 2, 10). Interestingly, for some units the measured values differ significantly between the two wells. For the Jurassic layer, the extremes define a range of 2.5-3.1 $Wm^{-1}K^{-1}$, while for the Keuper layer the difference between the minimum and maximum is

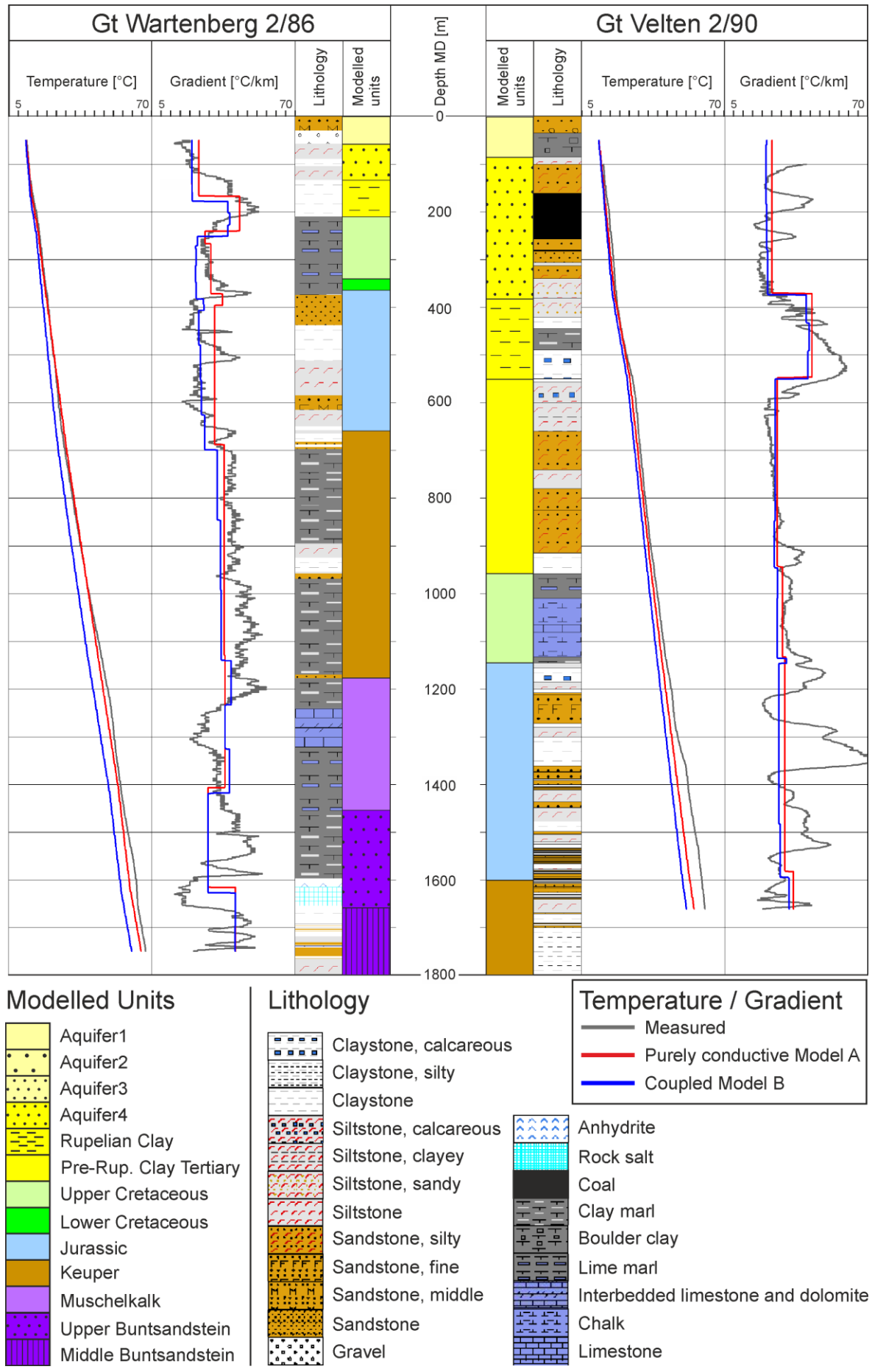

Fig 10 Measured and modelled temperatures, temperature gradients, lithologies and modelled geological units at the wells Gt Berlin-Wartenberg 2/86 and Gt Velten 2/90.

even wider (2.0-3.9 $Wm^{-1}K^{-1}$). Similarly, log-derived thermal conductivity from the "Stralsund" borehole, located about 200 km north of Berlin at the margin of the NEGB, also reveals maximum differences in formation values of about 1.0 $Wm^{-1}K^{-1}$ (Fuchs and Förster 2010).

These observations of significant differences between temperature-log derived thermal conductivities at different locations within the same stratigraphic unit supports the conclusion of recent studies that large variations in thermal conductivity are the result of lateral changes in sedimentary facies (Norden and Förster 2006; Schütz et al. 2013).

In addition to these lateral changes in lithology and thermal properties, there are also indications for vertical variations within the units that are not yet considered by the current parameterisation of the models. The temperature logs of *Velten* and *Wartenberg* show large changes in geothermal gradients within single units, such as the Jurassic, pointing to internal variations in the thermal properties (Fig. 10). However, for a Berlin-wide representation of corresponding sub-units with more homogeneous lithological and thermal properties, a larger database than currently available would be required. Hence, the thermal conductivity values used for modelling (Tab. 2) correspond to averages over the complete temperature log intersecting a unit.

Table 4 Minimum, maximum and mean temperatures predicted by the models for different depth levels

Elevation [m.a.s.l.]	Temperature [°C]					
	Model A			Model B		
	min	max	mean	min	max	mean
-1000	35	50	43	25	48	37
-2000	65	87	80	60	87	74
-3000	91	112	104	85	110	98
-4000	119	142	133	110	140	125
-6000	189	216	205	-	-	-

m.a.s.l.: metres above sea level

Calculating bulk thermal conductivities inversely from local heat flow density and log-derived interval temperature gradients (Blackwell and Steele 1989; Fuchs and Förster 2010) holds the advantage of obtaining *in-situ* values directly from the Berlin subsurface. Depending on the geological unit, these thermal-conductivity values may to a greater or lesser extent deviate from values reported by other studies in the NEGB. Norden et al. (2012) have reviewed existing literature from the basin and complemented this database by new laboratory measurements to characterise the whole sedimentary succession of a region some 100 km west of Berlin. For most units, the log-derived bulk thermal conductivity from the Berlin subsurface deviate by less than 10% from the conductivities proposed by Norden et al. (2012). Exceptions are the Cenozoic Aquifers 1-4 and the pre-Rupelian Tertiary unit, all being characterised by thermal conductivity values that are significantly larger in the two wells of Berlin than in other parts of the NEGB. This might indicate

that these units on average are richer in sandstone in the Berlin area, since sand- (quartz-) dominated clastics typically show higher matrix thermal conductivities than clay-rich clastics. One alternative explanation could be the surface heat flow that has been assumed to be constant across the area, although heat flow variations are likely because of the existence of salt diapirs locally reaching close to the surface.

Another potential explanation would be an inherited paleoclimatic effect, induced by lower surface temperatures during the Pleistocene ice ages and responsible for reduced thermal gradients in the shallow subsurface at present-day (e.g. Clauser et al. 1997; Norden et al. 2008; Šafanda and Rajver 2001; Šafanda et al. 2004). A related non-equilibrium of the measured temperature logs, i.e. temperature gradients lower than in thermal equilibrium, would lead to erroneously high thermal conductivities (Fourier's law). Generally, a transient model implementing the paleoclimatic temperature changes would improve representations of the present-day thermal field (Kukkonen and Jõeleht 2003; Kukkonen and Safanda 1996). Nevertheless, given the lack of direct information on the affected depth and related temperature shifts in the study area, we refrain from considering this subject at the current stage of geothermal exploration. This is also because most of the main changes in geothermal gradients are already reliably reproduced by the modelled gradients (Fig. 10). For example, increased temperature gradients observed at ~100-250 m depth at *Wartenberg* and at ~380-600 m depth at *Velten* and reflecting changes in lithological composition appear also in the models. They can clearly be attributed to the Rupelian Clay unit, of which the thermal conductivity is smaller compared to rocks below and above (Tab. 2) and thus induces a more efficient heat storage and higher temperature gradients below. Even if the models do not reproduce all of the larger changes in thermal gradients, as within the Jurassic unit of the well *Velten* (Fig. 10), these deviations must be related to not yet implemented lithological differentiations within the sequence (Fig. 10). Thus, the next steps of the exploration campaign should focus on integrating (as soon as available) more information on changes in facies and physical rock properties.

6.3 Influence of moving fluids

The overall goal of this study is to consider all processes contributing to the internal heat budget of the study area, while quantifying the effects of the different parameters involved. Therefore, the calculated lithosphere-scale temperature conditions were used as a starting point for complementary and more detailed simulations of coupled fluid and heat transfer (down to 6,000 m depth; Model B). The second model thus takes into account transient effects on temperatures due to moving groundwater. The relative impact of different heat transport mechanisms on the thermal field of the NEGB has been demonstrated before (e.g. Kaiser et al. 2011). Also for the Perth metropolitan area, the consideration of coupled fluid and heat transport has been shown to be essential to estimate the

exploitable heat in place (Schilling et al. 2013). In this hydrogeologically and tectonically complex setting, both topography-driven advection and free convection create thermal anomalies of much shorter distances than would be related to the conductive thermal field. Similarly, by comparing a purely conductive reference model with measured temperatures and by developing complementary type models for coupled fluid and heat transport, Rühaak et al. (2010) assumed free convection within faults as the cause for observed positive thermal anomalies in the western Molasse Basin.

For comparability, the set-up of the purely conductive Model A and the coupled Model B has been maintained consistent when possible, i.e. in terms of the 3D geologic structure, thermal conductivities, radiogenic heat production, and boundary conditions. As a consequence, the computed results show some important similarities that are related to the effects of conductive heat transport such as those thermal anomalies induced by the complex geometry of the highly conductive Zechstein salt layer. However, any differences between the results of the purely conductive and the coupled models are a quantitative expression of the effect of groundwater flow on the temperature distribution.

Most obviously, the coupled Model B predicts colder temperatures on average than the purely conductive Model A as can been seen from the temperature variations at constant depth levels (Fig. 5, 6). Also the thermal gradients of Model A are larger than those of Model B, at least down to depths of 1,200 m at the well *Wartenberg* and down to 550 m at *Velten* (Fig. 10). Even though the negative thermal anomalies may originate at relatively shallow levels, due to the overall thermal balance required by physical reasons, they propagate deeper, thus explaining the overall negative shift of temperatures in the coupled model at greater depths (8°C at 4000 m depth; Tab. 4). However, the groundwater induced cooling effect might be overestimated in the coupled models as a consequence of both an oversimplified upper flow boundary condition and oversimplified shallow aquifer-aquitard structure. The modelled hydraulic head defined as a subdued replica of the surface topography enables to account for first order features of regional flow, i.e. locations of major recharge and discharge areas. However, it implies unrealistically high values for the imposed surface pressure. This in turn may lead to solving for an "overstressed" surface water infiltration flow component. A by-product of this groundwater dynamics is that areas of direct infiltration will observe an oversupply of surface water leading to a stronger cooling in the underground.

The groundwater flow induced cooling effect has been found to vary according to the hydrogeological setting of the sedimentary sequences. In this regard, the geometry of the Tertiary Rupelian layer, which constitutes the most effective and shallowest regional hydraulic barrier, comes into play (Fig. 3b, Fig. 4a). A stronger cooling effect and thus larger differences between simulated temperatures between the two model realisations are found in spatial correlation with the Rupelian hydrogeological windows (Fig. 3b, Fig. 6c), i.e. where this aquitard is not hampering the

downward flow of colder fluids. This groundwater induced cooling effect of the subsurface and its lateral variability due to the discontinuous distribution of the low-permeable Rupelian Clay has also been proposed for other parts of the NEGB (Magri et al. 2008; Noack et al. 2013 - this issue).

The correlation between the topography of the area (Fig. 3a) and the temperature differences between the purely conductive and coupled models (Fig. 6b) demonstrates the impact of topography-driven forced convection on the thermal field. In contrast, we do not find indications for density and buoyancy-driven free convection of the modelled fluids. This is in agreement with the results of Kaiser et al. (2011) and Noack et al. (2013 - this issue). They show that conditions facilitating free convection are rarely met within the NEGB and that free convection will be suppressed where the hydraulic potential is high, so that the thermal signature of the system is controlled rather by the forced convective flow components.

Although the coupled model is more complete and thus more realistic in terms of the physics considered, the absolute temperatures predicted by the purely conductive model are closer to the observed values across the available temperature logs (Fig. 10). We take this as another indication for a parameterisation that still must be improved. It is well known that the main Quaternary to upper Tertiary aquifers under Berlin are extensively intercalated by glacial till and boulder clay layers. Depending on the geometric alternation of such aquitards and aquifers, different groundwater-flow conditions may be locally realised (from confined to perched or even phreatic groundwater flow). This has an additional impact on the interactions between surface and deeper water as well as on the resulting temperature distribution with depth, an impact that cannot be reflected by our current models. Therefore, to increase the accuracy of the numerical simulations calls for more detailed information on the geometries and properties of the major hydrogeological units.

Despite the mentioned uncertainties in parameterisation, the average misfit between modelled and available measured temperatures is minor (Fig. 10). For Model A, predicted temperatures deviate by -1.0°C on average from the well temperatures at *Velten*, and by 1.1°C from the temperatures at *Wartenberg*. For Model B, the average deviation is -6.7°C at *Wartenberg* and -4.5°C at *Velten*. Although these two temperature logs provide control only about the uppermost 2 km of the subsurface, we regard the consistency between modelling results and observations as validating the general model set-up. Hence, the modelled temperature distributions are suitable for an analysis of the related controlling factors and for first statements on the deep geothermal potential of the city.

7 Conclusions

1. *The models predict significant lateral temperature variations for the subsurface of Berlin.*

These variations are induced by physical properties changing spatially according to a complex 3D structure of the geological units. Thereby, the geometries of the highly conductive Zechstein salt layer and of the hydraulically impervious Rupelian Clay layer are of major importance.

2. *The relevance of the models arises from the integration of physics and local observations.*

The developed 3D structural model of Berlin is consistent with the complex regional geological setting and local borehole observations. It allows representing the subsurface in terms of thermal and hydraulic properties most of which are derived from laboratory or *in-situ* measurements. Numerical simulations of interacting heat transport mechanisms result in temperature predictions that are validated by temperature measurements from the area.

3. *The models are useful additions for the virtual Energy Atlas Berlin.*

Potential geothermal reservoirs such as the Middle Buntsandstein and the Sedimentary Rotliegend can be visualised according to their subsurface geometries and temperature distributions. Similarly, economically relevant isotherms as predicted by the 3D models can be integrated into the virtual city where they will directly be linked to information on energy demand and infrastructure.

4. *The models provide a suitable base for the further decision-making process.*

The next steps in the assessment of the geothermal potential of the city should focus on the reservoir scale and the dynamic behaviour of hydraulically enhanced systems. The results of this study assist with identifying areas of geothermal interest for further numerical simulations, geophysical exploration, or drilling.

5. *Subsequent numerical simulations will require more in-situ data.*

Most of the thermal conductivities adopted in the models represent *in-situ* values from the Berlin area, which is an improvement compared to earlier studies in the region and an explanation for the comparably good fit between measured and modelled temperatures. However, so far the validation of the thermal models relies on only two wells with available temperatures from depths of less than 2,000 m. Moreover, the largest deviations of the models are caused by a lack in detailed knowledge about the spatial variations of lithologies and related thermal and hydraulic properties.

Acknowledgements

We would like to thank GTN Geothermie Neubrandenburg, LBGR Brandenburg, Senatsverwaltung Berlin, and GASAG Berlin for their support and for providing diverse data sets including core data and drilling reports. Especially, we would like to acknowledge Berliner Erdgasspeicher GmbH for allocating stratigraphic information from the well *E Berlin 1/70*. Many thanks go also to Inga Moeck for fruitful discussion on the Berlin subsurface geology and to Christoph Wehner for his technical help in completing this manuscript. This study was co-funded by the European Union in the framework of the Climate Knowledge and Innovation Centre of the European Institute of Technology (EIT Climate-KIC) projects Energy Atlas Berlin and Neighbourhood Demonstraters.

References

Agemar T, Schellschmidt R, Schulz R (2012) Subsurface temperature distribution in Germany. Geothermics 44: 65-77.

Balling P, Maystrenko YP, Scheck-Wenderoth M (2013, this issue) The deep thermal field of the Glueckstadt Graben. Environmental Earth Sciences.

Bayer U, Scheck M, Koehler M (1997) Modeling of the 3D thermal field in the Northeast German Basin. Geologische Rundschau (International Journal of Earth Sciences) 86: 241-251.

Bear J (1979) Hydraulics of Groundwater. McGraw-Hill, New York

Benek R, Kramer W, McCann T, Scheck M, Negendank JFW, Korich D, Huebscher HD, Bayer U (1996) Permo-carboniferous magmatism of the Northeast German Basin. Tectonophysics 266: 379-404.

Berliner Senatsverwaltung für Wirtschaft, Technologie und Frauen (2011) Energiekonzept 2020, Langfassung, Energie für Berlin, Effizient - Erneuerbar - Zukunftsfähig. Berliner Senatsverwaltung für Wirtschaft, Technologie und Frauen

Blackwell DD, Steele JL (1989) Heat flow and thermal potential of Kansas. In: Steeples DW (ed) Geophysics in Kansas, vol 226. Kansas Geological Survey Bulletin, pp 267-295

Blöcher MG, Zimmermann G, Moeck I, Brandt W, Hassanzadegan A, Magri F (2010) 3D numerical modeling of hydrothermal processes during the lifetime of a deep geothermal reservoir. Geofluids 10: 406-421.

Cacace, M., Kaiser, B.O., Lewerenz, B., Scheck-Wenderoth, M., 2010. Geothermal energy in sedimentary basins: What we can learn from regional numerical models. Chemie der Erde - Geochemistry 70, 33-46.

Cacace M, Blöcher MG, Watanabe N, Moeck I, Börsing N, Scheck-Wenderoth M, Kolditz O, Huenges E (2013) Modelling of Fractured Carbonate Reservoirs - Outline of a novel technique via a case study from the Molasse Basin, southern Bavaria (Germany). Environmental Earth Sciences. doi: DOI 10.1007/s12665-013-2402-3

Cherubini Y, Cacace M, Scheck-Wenderoth M, Moeck I, Lewerenz B (2013) Controls on the deep thermal field - implications from 3D numerical simulations for the geothermal research site Groß Schönebeck. Environmental Earth Sciences. doi: 10.1007/s12665-013-2519-4

Clauser C, Giese P, Huenges E, Kohl T, Lehmann H, Rybach L, Å afanda J, Wilhelm H, Windloff K (1997) The thermal regime of the crystalline continental crust: Implications from the KTB. Journal of Geophysical Research 102 (B8): 18417-18441.

Diersch H-J (2009) FEFLOW Finite Element Subsurface Flow & Transport Simulation System, Reference Manual. WASY GmbH Institute for Water Resources Planning and System Research, Berlin

FIG Commission 3 (2010) Rapid Urbanization and Mega Cities: The Need for Spatial Information Management, Research study by FIG Commission 3 In: Potsiou C (ed) FIG Publication, vol 48. The International Federation of Surveyors (FIG), Copenhagen (Denmark) pp 90

Fuchs S, Förster A (2010) Rock thermal conductivity of Mesozoic geothermal aquifers in the Northeast German Basin. Chemie der Erde - Geochemistry 70: 13-22.

Henning A, Limberg A (2012) Variation of the subsoil temperature field in Berlin as a result of climate change and urbanization. Brandenburgische Geowissenschaftliche Beiträge, Cottbus 19: 81-92.

Hoth K, Rusbült J, Zagora K, Beer H, Hartmann O (1993) Die tiefen Bohrungen im Zentralabschnitt der Mitteleuropäischen Senke - Dokumentation für den Zeitabschnitt 1962-1990. Gesellschaft für Geowissenschaften Berlin

Huenges E (2010) Geothermal Energy Systems: Exploration, Development and Utilization. Wiley-VCH

Hurtig E, Rockel W (1992) Federal Republic of Germany Eastern Federal States. In: Hurtig E, Cermak V, Heanel R, Zui V (eds) Geothermal atlas of Europe Hermann Haack Verlagsgesellschaft mbH, Gotha, pp 38-40

Jaroch A (2006) Stratifizierung des hydrogeologischen 3D Modells von Berlin unter Berücksichtigung qualifizierter Bohrungsinformationen. Unpublished master thesis Technical University of Berlin

Jensen PK (1990) Analysis of the temperature field around salt diapirs Geothermics 19: 273-283.

Kaiser BO, Cacace M, Scheck-Wenderoth M, Lewerenz B (2011) Characterization of main heat transport processes in the Northeast German Basin: constraints from 3-D numerical models. Geochemistry, Geophysics, Geosystems 12: 17.

Kastner O, Sippel J, Scheck-Wenderoth M, Huenges E (2013, this issue) The deep geothermal potential of the Berlin area. Environmental Earth Sciences

Kukkonen IT, J õeleht A (2003) Weichselian temperatures from geothermal heat flow data. Journal of Geophysical Research: Solid Earth 108 (B3): 2163.

Kukkonen IT, Šafanda J (1996) Palaeoclimate and structure: the most important factors controlling subsurface temperatures in crystalline rocks. A case history from Outokumpu, eastern Finland. Geophysical Journal International 126: 101-112.

LIAG (2009) Geophysics Information System. http://www.liag-hannover.de/en/research-of-methods-sections/geothermics-information-systems/projects/fis-gp-geophysics-information-system.html

Magri F, Bayer U, Tesmer M, Möller P, Pekdeger A (2008) Salinization problems in the NEGB: results from thermohaline simulations. International Journal of Earth Sciences (Geologische Rundschau) 97.

Maystrenko Y, Bayer U, Scheck-Wenderoth M (2013) Salt as a 3D element in structural modeling - Example from the Central European Basin System. Tectonophysics 591: 62-82. doi: 10.1016/j.tecto.2012.06.030

Maystrenko YP, Scheck-Wenderoth M (2013) 3D lithosphere-scale density model of the Central European Basin System and adjacent areas. Tectonophysics in press (accepted manuscript, available online 27 April 2013). doi: 10.1016/j.tecto.2013.04.023

Mottaghy D, Pechnig R, Vogt C (2011) The geothermal project Den Haag: 3D numerical models for temperature prediction and reservoir simulation. Geothermics 40: 199-210.

Nield DA, Bejan A (2006) Convection in Porous Media. Springer

Noack V, Cherubini Y, Scheck-Wenderoth M, Lewerenz B, Höding T, Simon A, Moeck I (2010) Assessment of the present-day thermal field (NE German Basin) - Inferences from 3D modelling. Chemie der Erde 70: 47-62.

Noack V, Scheck-Wenderoth M, Cacace M (2012) Sensitivity of 3D thermal models to the choice of boundary conditions and thermal properties: a case study for the area of Brandenburg (NE German Basin). Environmental Earth Sciences 67 (6): 1695-1711. doi: 10.1007/s12665-012-1614-2

Noack V, Scheck-Wenderoth M, Cacace M, Schneider M (2013) Influence of fluid flow on the regional thermal field: results from 3D numerical modelling for the area of Brandenburg (North German Basin) Environmental Earth Sciences. doi: DOI 10.1007/s12665-013-2438-4

Norden B, Förster A (2006) Thermal conductivity and radiogenic heat production of sedimentary and magmatic rocks in the Northeast German Basin. AAPG Bulletin 90: 939-962.

Norden B, Förster A, Balling N (2008) Heat flow and lithospheric thermal regime in the Northeast German Basin. Tectonophysics 460: 215-229.

Norden B, Förster A, Behrends K, Krause K, Stecken L, Meyer R (2012) Geological 3-D model of the larger Altensalzwedel area, Germany, for temperature prognosis and reservoir simulation. Environmental Earth Sciences 67 (2): 511-526. doi: 10.1007/s12665-012-1709-9

Philipp SL, Parchwitz S, Götz AE (2011) Geothermal Potential of the Upper Muschelkalk in Northeastern Germany. EGU General Assembly, vol 13, EGU2011-2487. EGU 2011, Vienna (Austria)

Pöppelreiter M, Borkhataria R, Aigner T, Pipping K (2005) Production from Muschelkalk carbonates (Triassic, NE Netherlands): unique play or overlooked opportunity? Geological Society, London, Petroleum Geology Conference series 6: 299-315. doi: 10.1144/0060299

Rühaak W, Rath V, Clauser C (2010) Detecting thermal anomalies within the Molasse Basin, southern Germany. Hydrogeology Journal 18: 1897-1915.

Šafanda J, Rajver D (2001) Signature of the last ice age in the present subsurface temperatures in the Czech Republic and Slovenia. Global and Planetary Change 29: 241-257.

Šafanda J, Szewczyk J, Majorowicz J (2004) Geothermal evidence of very low glacial temperatures on a rim of the Fennoscandian ice sheet. Geophysical Research Letters 31: L07211.

Scheck M, Bayer U (1999) Evolution of the Northeast German Basin - inferences from a 3D structural model and subsidence analysis. Tectonophysics 313: 145-169.

Scheck M, Bayer U, Lewerenz B (2003) Salt movement in the Northeast German Basin and its relation to major post-Permian tectonic phases - results from 3D structural modelling, backstripping and reflection seismic data Tectonophysics 361: 277-299.

Scheck-Wenderoth M, Lamarche J (2005) Crustal memory and basin evolution in the Central European Basin System - new insights from a3D structural model. Tectonophysics 397: 132-165.

Schilling O, Sheldon HA, Reid LB, Corbel S (2013) Hydrothermal models of the Perth metropolitan area, Western Australia: implications for geothermal energy. Hydrogeology Journal 21: 605-621.

Schütz F, Fuchs S, Förster A, Förster H-J Facies-related trends of rock thermal conductivity and the impact on temperature prognosis for geothermal target reservoirs General Assembly European Geosciences Union 2013, Vienna, Austria (07-12 April 2013) 2013. Geophysical Research Abstracts 15 (EGU2013-3187)

Stackebrandt W, Manhenke V (2002) Atlas zur Geologie von Brandenburg im Maßstab 1:1000000. Landesamt für Geowissenschaften und Rohstoffe, Kleinmachnow

Wong LW, Watanabe N, Cacace M, Blöcher MG, Kastner O, Zimmermann G (2013, this issue) Sensitivity analysis of permeability and apertures of natural internal fault zones on fluid flow and heat transfer in a deep geothermal reservoir. Environmental Earth Sciences.